RESEARCH ARTICLE

Chemotaxis–Reaction Models in Microbial Ecology: Theory, Analysis, and Applications

Kolade M. Owolabi[1,2,*], **Eben Maré**[3] and **Clara O. Ijalana**[1]

[1] Department of Mathematical Sciences, Federal University of Technology Akure, PMB 704, Akure, Ondo State, Nigeria
[2] Department of Mathematics and Applied Mathematics, School of Science and Technology, Sefako Makgatho Health Sciences University, Ga-Rankuwa 0208, South Africa
[3] Department of Mathematics and Applied Mathematics, University of Pretoria, Pretoria 002, South Africa

Abstract

Chemotaxis, the directed movement of microorganisms in response to chemical gradients, plays a pivotal role in microbial ecology. This article provides a comprehensive review of mathematical models that couple chemotaxis with reaction dynamics to describe microbial population behavior. We discuss how such chemotaxis–reaction models capture essential ecological phenomena, from nutrient foraging and biofilm formation to inter-species competition and environmental processes. Key model formulations, starting from the classical Keller–Segel system, are presented alongside extensions incorporating multiple species, complex reaction terms, and fluid flow coupling. We survey rigorous mathematical results on well-posedness, pattern formation, and stability, highlighting analytical tools in partial differential equations (PDEs) and functional analysis. Numerical simulation techniques are reviewed, illustrating how computational methods can capture chemotactic pattern formation. Biological applications are emphasized throughout, drawing connections between model predictions and experimental observations of bacterial aggregation patterns, biofilm spatial structure, and microbial competition. Finally, we outline open problems and future directions, including stochastic modeling, multiscale approaches, and data-driven techniques, underscoring the interdisciplinary outlook. The contributions of this article lie in synthesizing recent advances in chemotaxis–reaction modeling and analysis, and in elucidating the interplay between theory and experiment in microbial ecology.

Keywords: Keller-Segel model, Chemotaxis, reaction-diffusion systems, lyapunov stability, pattern formation, nonlinear PDEs, microbial ecology.

1 Introduction

Microorganisms exhibit remarkable collective behaviors that profoundly influence ecological, biomedical, and environmental systems. One of the most important of these behaviors is *chemotaxis*, the directed movement of motile cells along chemical concentration gradients. Chemotaxis enables bacteria and other microorganisms to locate nutrients, avoid toxins, coordinate multicellular activity, and adapt to dynamically changing environments. These processes

Submitted: 29 March 2026
Accepted: 22 May 2026
Published: 27 May 2026

Vol. 2, **No.** 2, 2026.
10.62762/JNDA.2026.783618

***Corresponding author:**
✉ Kolade M. Owolabi
mkowolax@yahoo.com; kmowolabi@futa.edu.ng

Citation
Owolabi, K. M., Maré, E., & Ijalana, C. (2026). Chemotaxis–Reaction Models in Microbial Ecology: Theory, Analysis, and Applications. *Journal of Nonlinear Dynamics and Applications*, 2(2), 76–107.

are central to microbial survival and ecological organization, influencing nutrient cycling in soils, marine microbial ecology, infection dynamics, tumor invasion, wound healing, and biofilm development [1–3]. Recent experimental and computational studies have further demonstrated that chemotactic interactions can generate highly complex collective behaviors, including aggregation, wave propagation, spatial self-organization, quorum-dependent migration, and emergent pattern formation in heterogeneous environments [4–7].

Mathematical modeling provides a rigorous framework for linking microscopic microbial movement mechanisms with macroscopic population-level dynamics. In particular, partial differential equation (PDE) models combining chemotaxis with reaction kinetics — commonly referred to as *chemotaxis–reaction systems* — have become a foundational tool in mathematical biology and microbial ecology [2, 3, 8, 9]. These models extend classical reaction–diffusion equations by incorporating directed drift terms that represent biased movement toward or away from chemical signals. Such frameworks are capable of describing a wide range of biologically relevant phenomena, including bacterial aggregation into high-density clusters, traveling pulse formation, spatial segregation of competing microbial populations, chemotaxis-driven invasion processes, biofilm initiation, and ecological adaptation under nutrient-limited conditions.

Among the most influential mathematical frameworks is the classical Keller–Segel model introduced by Keller and Segel in the early 1970s [2, 8]. Since its introduction, the Keller–Segel system has served as a prototype nonlinear PDE model for studying chemotactic aggregation, diffusion-driven instability, blow-up phenomena, and pattern formation. Extensive mathematical research has been devoted to understanding the qualitative behavior of Keller–Segel-type systems, including global existence, finite-time blow-up, boundedness, asymptotic stability, entropy structures, and bifurcation mechanisms [10–12]. More recently, modern developments have expanded the classical framework to include logistic growth, signal consumption, fluid coupling, stochastic forcing, volume-filling effects, degenerate diffusion, nonlocal interactions, and multiscale biological feedback mechanisms [13–16, 22].

Over the last several years, there has been renewed interest in chemotaxis modeling due to advances in experimental microbiology, imaging technologies, microfluidic platforms, and data-driven biological analysis. Modern studies increasingly combine mathematical analysis with high-resolution experiments and computational simulations to investigate chemotaxis in realistic ecological environments [17–19]. In particular, recent works between 2020 and 2026 have explored stochastic chemotaxis systems, chemotaxis–fluid interactions, machine-learning-assisted parameter inference, hybrid agent-based/PDE frameworks, and multiscale microbial dynamics in porous and heterogeneous media [7, 20, 21]. These developments highlight the growing importance of integrating rigorous mathematical theory with computational and experimental approaches.

At the same time, important theoretical challenges remain unresolved. Chemotaxis systems are strongly nonlinear and may exhibit singularity formation, metastability, multiscale pattern evolution, and parameter-sensitive dynamics that are difficult to analyze rigorously. While substantial progress has been achieved for simplified Keller–Segel models, many biologically realistic systems remain mathematically poorly understood, especially in higher spatial dimensions or in the presence of stochasticity, fluid transport, and heterogeneous environmental effects [9, 14, 15]. Furthermore, the growing use of numerical simulation and data-driven biological modeling has generated renewed interest in stable, positivity-preserving, and adaptive computational methods for chemotaxis PDEs [4, 16, 21].

The primary objective of this review is to provide a modern and mathematically integrated synthesis of chemotaxis–reaction modeling in microbial ecology while connecting biological interpretation, nonlinear PDE analysis, computational methodology, and emerging data-driven approaches. Although several important reviews and monographs on chemotaxis theory already exist [3, 9–11], many earlier surveys focus predominantly on either biological phenomenology, classical Keller–Segel analysis, or isolated mathematical aspects such as blow-up theory and pattern formation. In contrast, the present review emphasizes the simultaneous interaction between modern analytical theory, ecological applications, computational methods, and recent multiscale developments.

More specifically, the novelty of this review

lies in several complementary directions. First, we integrate classical chemotaxis theory with recent advances involving stochastic chemotaxis systems, chemotaxis–fluid coupling, multiscale ecological interactions, hybrid PDE–agent frameworks, machine-learning-assisted parameter inference, and adaptive numerical stabilization methods. Second, unlike many earlier reviews that treat mathematical analysis and biological interpretation separately, we consistently connect analytical results with experimentally observed microbial behaviors such as aggregation, quorum-dependent migration, traveling bands, biofilm formation, and ecological spatial organization. Third, we provide a unified discussion that combines rigorous PDE theory, computational methodology, and ecological interpretation within a single framework intended for researchers across applied mathematics, computational science, microbiology, and ecological modeling.

To improve clarity and avoid ambiguity regarding the role of different materials presented in this manuscript, we explicitly distinguish between established theoretical results from the literature and illustrative material included for pedagogical purposes. Classical existence theorems, blow-up criteria, stability results, and foundational Keller–Segel formulations are presented as part of the established mathematical literature and are appropriately referenced throughout. By contrast, certain derivations, simplified analytical examples, schematic computational illustrations, and explanatory nondimensionalization procedures included in Sections 4 and 5 are intended primarily to clarify modeling ideas and provide intuition for readers entering the field. These illustrative components are not presented as new mathematical theorems unless explicitly stated otherwise.

In addition, to facilitate comparison between different chemotaxis frameworks, we include a consolidated summary of major model classes, their principal assumptions, mathematical structures, and representative ecological applications. This comparative perspective is intended to help readers identify the appropriate modeling framework for particular biological scenarios while also highlighting the mathematical trade-offs between analytical tractability and biological realism.

The paper is organized as follows. Section 2 presents biological background on microbial chemotaxis, signaling mechanisms, and ecological interactions in order to motivate the mathematical formulations. Section 3 introduces the classical Keller–Segel framework and discusses important extensions involving multiple species, chemotaxis–reaction coupling, logistic growth, nonlocal interactions, stochastic effects, and fluid transport mechanisms. In Section 4, we examine the mathematical analysis of chemotaxis systems, including well-posedness, boundedness, blow-up phenomena, stability theory, pattern formation, and bifurcation analysis. We also review major numerical approaches, including finite difference, finite element, adaptive mesh, positivity-preserving, hybrid particle-based, and multiscale computational methods.

Biological insights and applications are interwoven throughout the manuscript. In particular, we discuss bacterial aggregation and self-organization phenomena, including experimentally observed spot and ring patterns in *E. coli* and related microbial systems [23]. Additional applications include biofilm development, microbial competition, ecological invasion, chemotaxis-driven nutrient acquisition, and environmental bioremediation processes. We further emphasize the growing importance of experimental validation, parameter estimation, uncertainty quantification, and computational reproducibility in modern chemotaxis research.

Section 5 presents supplementary theoretical developments and model derivations, including nondimensionalization, derivation of chemotactic fluxes from biased random walks, and illustrative analytical examples intended to clarify the mathematical mechanisms underlying chemotactic aggregation. Section 6 discusses open problems and future research directions, including stochastic chemotaxis modeling, machine-learning-assisted PDE analysis, multiscale ecological systems, uncertainty quantification, and coupling between chemotaxis, fluid transport, and intracellular signaling dynamics. Finally, Section 7 concludes the paper with a synthesis of major insights and perspectives for future interdisciplinary research.

Throughout this review, we aim to balance mathematical rigor with biological relevance. All mathematical formulations are presented using precise scientific language appropriate for mathematical biology and nonlinear PDE research, while maintaining sufficient biological context to ensure accessibility for interdisciplinary readers from applied mathematics, computational science, ecology, and microbiology.

Table 1. Comparison of major chemotaxis–reaction model classes, their assumptions, and representative applications.

Model Class	Main Assumptions	Mathematical Features	Representative Applications
Classical Keller–Segel models	Single-species chemotactic aggregation toward a chemical signal	Nonlinear PDE system with diffusion and chemotactic drift; possible blow-up and pattern formation	Bacterial aggregation, slime mold chemotaxis, traveling bands
Logistic chemotaxis models	Population growth limited by environmental carrying capacity	Additional logistic damping terms improve boundedness and global existence	Population regulation, nutrient-limited microbial growth
Multi-species chemotaxis systems	Several interacting microbial populations compete or cooperate	Coupled nonlinear PDE systems with multiple taxis mechanisms	Microbial competition, ecological coexistence, spatial segregation
Chemotaxis–fluid models	Microbial movement occurs within flowing fluids	Coupling between Keller–Segel dynamics and Navier–Stokes equations	Bioconvection, aquatic microbial transport, porous media flow
Nonlocal and volume-filling models	Finite-size effects and long-range interactions influence movement	Nonlocal interaction kernels and density-dependent chemotactic sensitivity	Crowded biofilms, tissue-scale aggregation
Stochastic chemotaxis models	Environmental fluctuations and random effects influence dynamics	Stochastic PDEs or probabilistic transport equations	Heterogeneous environments, noisy microbial dynamics
Hybrid and multiscale models	Discrete cellular behavior interacts with continuum fields	Coupled agent-based and PDE frameworks	Biofilm architecture, intracellular signaling, multiscale ecology
Data-driven and machine-learning-assisted models	Experimental data guide parameter estimation and prediction	PINNs, inverse problems, data assimilation, surrogate modeling	Parameter inference, computational biology, predictive microbial ecology

Summary of Major Chemotaxis–Reaction Model Classes

Table 1 summarizes the principal classes of chemotaxis–reaction models discussed throughout this review, together with their core assumptions, mathematical structures, and representative biological applications.

2 Biological Background and Modeling Motivation

Chemotaxis is the directed movement of cells or microorganisms in response to chemical gradients. In microbial systems, chemotactic motion enables organisms to locate nutrients, avoid harmful substances, coordinate collective behavior, and adapt to heterogeneous environments. Unlike purely diffusive motion, chemotaxis introduces directional bias into population transport, thereby generating nonuniform spatial distributions and complex spatiotemporal dynamics.

Chemotactic behavior has been extensively observed across diverse microbial species. Classical examples include *Escherichia coli*, which modulates its run-and-tumble motion in response to attractant gradients [1], and the social amoeba *Dictyostelium discoideum*, whose aggregation dynamics are coordinated through cyclic AMP signaling. Similar mechanisms arise in bacterial swarming, microbial colony expansion, biofilm initiation, and ecological migration processes. These systems demonstrate that chemotaxis can operate across multiple spatial and temporal scales, ranging from intracellular signaling to population-level pattern formation.

From a modeling perspective, chemotaxis is fundamentally important because it couples cellular movement with evolving chemical fields. Microorganisms both respond to and modify their chemical environment through nutrient consumption, signal secretion, toxin production, and metabolic activity. Consequently, microbial populations and chemical concentrations evolve through strongly coupled feedback mechanisms. This interaction naturally leads to systems of nonlinear partial differential equations involving:

- diffusive transport representing random motility,
- chemotactic drift terms describing biased movement along chemical gradients,
- reaction kinetics governing growth, decay, production, and consumption processes,

- and, in more realistic settings, fluid transport, stochastic effects, and multiscale interactions.

Chemotaxis also plays a central role in microbial ecology. In nutrient-limited environments, bacteria migrate toward localized nutrient sources, producing aggregation phenomena and traveling population bands. In multi-species communities, chemotactic responses may enhance competition, facilitate cooperative cross-feeding interactions, or generate spatial segregation between populations. Chemically mediated interactions further contribute to biofilm development, quorum sensing dynamics, ecological invasion, and microbial self-organization in heterogeneous environments.

These biological mechanisms motivate the development of chemotaxis–reaction systems capable of linking microscopic movement behavior with macroscopic population dynamics. The resulting mathematical models must account not only for directional migration, but also for nonlinear ecological feedbacks, pattern formation, and multiscale spatial organization. The next section introduces the classical Keller–Segel framework and several important modern extensions used in microbial ecology and mathematical biology.

3 Mathematical Modeling of Chemotaxis–Reaction Systems

Chemotaxis–reaction systems describe the coupled evolution of microbial populations and chemical signals through nonlinear partial differential equations. These models typically combine:

- diffusive transport representing random motility,
- chemotactic drift induced by chemical gradients,
- and reaction kinetics describing growth, decay, production, and consumption processes.

The foundational framework in chemotaxis theory is the Keller–Segel model introduced in the early 1970s [2, 8]. Since then, numerous extensions have been developed to incorporate ecological interactions, multiscale effects, fluid transport, stochasticity, and nonlinear regulatory mechanisms relevant to microbial ecology [9, 14, 15].

Let $n(\mathbf{x}, t)$ denote the microbial density and $c(\mathbf{x}, t)$ the concentration of a chemoattractant.

3.1 Classical Keller–Segel Model

The classical Keller–Segel system is given by

$$\partial_t n = D_n \Delta n - \chi \nabla \cdot (n \nabla c), \tag{1}$$
$$\partial_t c = D_c \Delta c + \alpha n - \beta c. \tag{2}$$

The diffusion term $D_n \Delta n$ models random cell motion, while the chemotactic flux $-\chi \nabla \cdot (n \nabla c)$ describes directed migration toward chemical gradients. The chemical field evolves through diffusion, cellular production, and natural degradation.

A widely studied reduction is the parabolic–elliptic Keller–Segel model obtained by assuming rapid chemical equilibration:

$$0 = D_c \Delta c + \alpha n - \beta c.$$

Despite its relatively simple structure, the Keller–Segel system exhibits rich nonlinear behavior including aggregation, diffusion-driven instability, pattern formation, and finite-time blow-up [10, 24]. In two spatial dimensions, the parabolic–elliptic model possesses a critical-mass phenomenon: solutions remain globally bounded below a threshold mass, while sufficiently large mass may lead to singular concentration [24].

The Keller–Segel framework has become a prototype model in nonlinear PDE analysis and mathematical biology, motivating extensive work on global existence, boundedness, entropy structures, and asymptotic dynamics [11, 12].

3.2 Generalized Chemotaxis Models

Biologically realistic microbial systems often require extensions of the classical Keller–Segel framework.

Multi-species systems. Multi-population models describe interacting microbial species with distinct chemotactic sensitivities and reaction kinetics:

$$\partial_t n_i = D_i \Delta n_i - \chi_i \nabla \cdot (n_i \nabla c) + f_i(n_1, \ldots, n_S),$$
$$i = 1, \ldots, S.$$

Such systems arise in microbial competition, ecological coexistence, predator–prey interactions, and spatial niche formation [25–27]. Recent studies have examined pattern formation, coexistence mechanisms, and cross-diffusion effects in multi-species Keller–Segel systems [14].

Multiple chemical signals and chemorepulsion. Many microorganisms respond simultaneously to attractants and repellents. This leads to models involving several chemical fields:

$$\mathbf{J} = -D_n \nabla n + \sum_k \chi_k n \nabla c_k.$$

These systems capture competing taxis mechanisms, toxin avoidance, and chemically mediated spatial organization.

Chemotaxis–fluid systems. In fluid environments, chemotaxis may couple with incompressible flow:

$$\begin{aligned} \partial_t n + \mathbf{u} \cdot \nabla n &= D_n \Delta n - \chi \nabla \cdot (n \nabla c), \\ \partial_t c + \mathbf{u} \cdot \nabla c &= D_c \Delta c + \alpha n - \beta c. \end{aligned}$$

Coupling with Navier–Stokes equations produces chemotaxis–fluid systems relevant to bioconvection, marine microbial transport, and porous-media ecology [28, 29]. Recent analytical work has focused on global weak solutions, stabilization, and fluid-driven pattern formation.

3.3 Reaction Mechanisms and Ecological Feedbacks

Reaction terms play a central role in regulating chemotactic aggregation and ecological dynamics.

Logistic growth. A common stabilization mechanism is logistic growth:

$$f(n) = rn\left(1 - \frac{n}{K}\right),$$

where K denotes the carrying capacity. Logistic damping suppresses excessive aggregation and often guarantees global boundedness [25].

Substrate-dependent growth. Microbial proliferation frequently depends on nutrient availability through Monod-type kinetics:

$$f(n, c) = \mu n \frac{c}{c + K_s}.$$

Such couplings generate feedback between nutrient consumption, chemotactic migration, and population growth, leading to traveling bands and wave-like aggregation phenomena.

Volume-filling and saturation effects. To account for crowding and finite-size constraints, chemotactic sensitivity may decrease at high density:

$$-\chi \nabla \cdot \left(n \left(1 - \frac{n}{n_{\max}}\right) \nabla c \right).$$

Volume-filling mechanisms prevent unrealistic concentration singularities and improve biological realism.

Toxin-mediated and inhibitory interactions. Additional chemical fields may represent toxins or inhibitory metabolites:

$$\partial_t w = D_w \Delta w + \eta n - \lambda w.$$

Such models describe chemically mediated competition, microbial exclusion zones, and antagonistic ecological interactions.

3.4 Recent Developments

Recent advances have significantly expanded the scope of chemotaxis modeling. Modern research increasingly incorporates stochastic effects, multiscale coupling, hybrid PDE–agent frameworks, and data-driven methodologies [30, 31].

Stochastic chemotaxis models account for environmental fluctuations and signaling noise through stochastic PDEs and random motility processes. Hybrid particle–continuum approaches combine agent-based dynamics with continuum chemical fields to capture microscale heterogeneity and collective behavior. Recent experimental advances involving microfluidics and AI-assisted imaging have also enabled high-resolution analysis of chemotactic migration in dynamically structured environments [32, 33].

These developments demonstrate the growing interaction between nonlinear PDE analysis, computational modeling, experimental microbiology, and ecological applications.

4 Mathematical Analysis and Modeling Perspectives

Chemotaxis–reaction systems generate a broad range of mathematical phenomena, including global regularity, finite-time blow-up, aggregation, pattern formation, and multiscale instability. The mathematical analysis of such systems has become a major research area in nonlinear PDE theory and mathematical biology [3, 9, 10, 15].

This section summarizes central analytical results for Keller–Segel-type models while explicitly distinguishing between rigorous classical theorems from the literature and simplified illustrative discussions included for exposition. We also discuss important limitations of continuum PDE chemotaxis models and clarify when PDE, agent-based, or multiscale approaches are most appropriate in microbial ecology applications.

4.1 Analytical Framework and Modeling Assumptions

Most rigorous results for chemotaxis systems rely on several standard assumptions:

- The microbial density and chemical concentrations are represented as continuous fields.
- Spatial domains are sufficiently smooth and bounded.
- Initial data are nonnegative and possess adequate regularity.
- Diffusion coefficients and chemotactic sensitivities are positive constants.
- Boundary conditions are typically homogeneous Neumann conditions, representing zero-flux boundaries.

These assumptions are mathematically convenient and biologically reasonable for sufficiently large populations in well-mixed or densely populated environments. However, they may become inaccurate in systems with strong stochasticity, low cell counts, intracellular heterogeneity, or discrete microscale interactions.

Unless otherwise stated, the theorems presented below summarize known results from the mathematical literature rather than new contributions of this review. We explicitly indicate the primary literature sources associated with each result.

4.2 Local and Global Well-Posedness

One of the first mathematical questions concerns whether solutions exist, remain unique, and preserve biological properties such as positivity.

Theorem 4.1 (Local Classical Solvability [10, 11]). *Let $\Omega \subset \mathbb{R}^d$ be a bounded smooth domain. Consider the classical Keller–Segel system*

$$\partial_t n = D_n \Delta n - \chi \nabla \cdot (n \nabla c), \tag{3}$$

$$\partial_t c = D_c \Delta c + \alpha n - \beta c, \tag{4}$$

subject to homogeneous Neumann boundary conditions and sufficiently regular nonnegative initial data

$$n_0, c_0 \in H^1(\Omega).$$

Then there exists a maximal time $T_{\max} > 0$ such that the system admits a unique nonnegative classical solution on $(0, T_{\max})$.

The proof relies on semigroup theory, parabolic regularity, and fixed-point arguments for the nonlinear chemotactic drift term. Analytically, the principal difficulty arises from the nonlinear coupling

$$\nabla \cdot (n \nabla c),$$

which combines transport and aggregation effects.

Biologically, local well-posedness ensures that the continuum model produces meaningful short-time population dynamics for sufficiently smooth initial microbial distributions.

A major question is whether solutions remain bounded for all time or develop singularities.

Theorem 4.2 (Global Boundedness with Logistic Damping [12, 14, 25]). *Consider the Keller–Segel system with logistic growth*

$$\partial_t n = D_n \Delta n - \chi \nabla \cdot (n \nabla c) + r n \left(1 - \frac{n}{K}\right), \tag{5}$$

$$\partial_t c = D_c \Delta c + \alpha n - \beta c. \tag{6}$$

Assume nonnegative bounded initial data and homogeneous Neumann boundary conditions. Then, under standard regularity assumptions, the system admits a unique global classical solution that remains uniformly bounded in time.

The stabilizing mechanism is the logistic damping term

$$-r n^2 / K,$$

which counteracts chemotactic aggregation and suppresses uncontrolled density growth.

This result is particularly important in microbial ecology because real microbial populations are constrained by nutrient limitation, crowding, and environmental carrying capacities. Consequently, logistic modifications are often more biologically realistic than the classical mass-conserving Keller–Segel model.

4.3 Blow-Up and Critical Mass Phenomena

One of the defining mathematical features of Keller–Segel systems is the possibility of finite-time blow-up, where cell density becomes unbounded.

Theorem 4.3 (Critical Mass Phenomenon in Two Dimensions [24, 34]). *For the classical parabolic–elliptic Keller–Segel system in $\mathbb{R}^2$, there exists a critical mass threshold*

$$M_c = 8\pi$$

(*in suitable nondimensional variables*) *such that:*

- *if the total mass satisfies $M < M_c$, solutions remain global;*
- *if $M > M_c$, finite-time blow-up may occur.*

This threshold reflects competition between:

- diffusion, which disperses cells;
- chemotactic aggregation, which concentrates cells.

From a biological viewpoint, blow-up represents extremely strong clustering behavior. Infinite densities are not physically realistic; instead, blow-up indicates breakdown of the continuum approximation and signals the need for additional biological mechanisms such as: volume-filling effects, finite-size exclusion, nutrient depletion, mechanical interactions, stochastic fluctuations.

Modern chemotaxis research therefore frequently augments Keller–Segel systems with regularizing mechanisms to prevent unrealistic singularities [14, 15].

4.4 Pattern Formation and Instability Mechanisms

Chemotaxis systems are well known for their ability to generate self-organized spatial structures.

Linear Instability Mechanism

Consider a homogeneous steady state (n^*, c^*). Linearization around this equilibrium and Fourier-mode analysis yield a dispersion relation for perturbation growth rates. Instability occurs when certain spatial modes satisfy

$$\mathrm{Re}(\lambda(k)) > 0.$$

For Keller–Segel-type systems, aggregation typically emerges when chemotactic attraction dominates diffusion and chemical decay. A simplified instability criterion is

$$\chi \alpha n^* > D_n \beta.$$

This mechanism is analogous to diffusion-driven instability in reaction–diffusion systems, although chemotactic transport rather than differential diffusion is the primary destabilizing factor.

Observed Pattern Structures

Rigorous analytical investigations and numerical simulations have demonstrated that chemotaxis systems can generate a wide variety of complex spatiotemporal structures, including aggregation spikes, traveling bands, spot and stripe-like patterns, propagating ring waves, and dynamically coarsening clusters. These emergent structures arise from the nonlinear interplay between chemotactic attraction, diffusion, reaction kinetics, and environmental heterogeneity. These structures have been observed experimentally in bacterial systems such as *E. coli* and *Bacillus subtilis* [23, 35].

4.5 Bifurcation and Stability Theory

Bifurcation analysis provides a systematic framework for understanding transitions between homogeneous and patterned states.

Turing-type bifurcation. As chemotactic sensitivity or chemical production increases beyond a threshold, homogeneous equilibria may lose stability and spatially heterogeneous steady states emerge.

Hopf bifurcation. Oscillatory dynamics in chemotaxis systems may emerge through Hopf bifurcation mechanisms when additional biological or physical effects are incorporated, including time delays, intracellular signaling feedback, predator–prey interactions, fluid coupling, or multiple interacting species. While classical Keller–Segel models typically produce stationary aggregation patterns, more general chemotaxis–reaction systems can exhibit sustained temporal oscillations, spatiotemporal periodic structures, and propagating wave behavior generated by the interaction between chemotactic transport, nonlinear reactions, and feedback mechanisms.

4.6 Limitations of the Keller–Segel Framework

Despite its mathematical importance, the Keller–Segel framework has several important limitations in microbial ecology.

1. **Continuum approximation.** The model assumes sufficiently large populations so that microbial densities can be treated as continuous fields. This becomes inaccurate when cell numbers are small or stochastic fluctuations dominate.

2. **Lack of intracellular signaling dynamics.** Classical Keller–Segel systems typically model only macroscopic movement and chemical transport, while neglecting receptor-level adaptation, signal transduction, and intracellular biochemical regulation.
3. **Simplified motility mechanisms.** Real microorganisms often exhibit run-and-tumble motion, persistence, anisotropic motility, or active mechanical interactions not fully captured by simple diffusion plus chemotactic drift.
4. **Unrealistic blow-up behavior.** Classical models may predict infinite densities, indicating missing biological regularization mechanisms.
5. **Limited environmental heterogeneity.** Many natural microbial habitats involve porous media, biofilms, fluid turbulence, and microscale spatial heterogeneity that exceed the assumptions of homogeneous continuum PDEs.
6. **Insufficient treatment of stochasticity.** Environmental fluctuations and random cellular responses can strongly influence microbial behavior, particularly in low-density systems.

These limitations have motivated the development of more advanced modeling frameworks, including stochastic chemotaxis formulations, agent-based and hybrid particle–continuum simulations, multiscale PDE systems, and data-driven approaches incorporating machine learning for parameter estimation, pattern prediction, and model calibration.

4.7 When Are PDE Models Appropriate?

An important modeling question concerns when continuum PDE descriptions are preferable to agent-based or multiscale approaches. PDE-based chemotaxis models are most effective when microbial populations are sufficiently large for continuum assumptions to remain valid and when the primary objective is to study collective spatial dynamics and averaged macroscopic behavior. They are particularly advantageous in situations where computational efficiency is important and where analytical insight into stability, bifurcation structure, aggregation thresholds, traveling waves, global boundedness, blow-up mechanisms, or large-scale ecological pattern formation is required. In this setting, continuum formulations provide a mathematically tractable framework capable of capturing diffusion, chemotactic transport, and nonlinear interactions over extended spatial and temporal scales.

In contrast, agent-based models become more appropriate when populations are sparse, stochastic fluctuations significantly influence the dynamics, or individual-cell behavior and intracellular signaling pathways must be explicitly resolved. Such discrete approaches are also better suited for modeling direct mechanical interactions, collisions, or heterogeneous cellular responses that cannot easily be represented within averaged continuum descriptions.

Multiscale and hybrid frameworks are preferable when microscopic cellular processes and macroscopic population dynamics strongly interact. This occurs, for example, when intracellular signaling pathways influence emergent colony-level behavior, when transport takes place in heterogeneous porous environments, or when simultaneous resolution of cellular and ecological scales is necessary. Recent developments increasingly integrate PDE analysis with stochastic simulation, agent-based modeling, and machine-learning-assisted parameter inference in order to combine analytical tractability with biological realism and data-driven calibration [30, 33].

5 Model Derivations and Nondimensionalization

5.1 Derivation of Chemotactic Flux

The classical Keller–Segel chemotaxis term can be derived from a biased random walk description of bacterial motion. Cells alternate between straight runs and random tumbles, and bias their motion by reducing tumbling frequency when moving toward higher chemical concentration.

Let $p(x,t)$ denote the cell density in one dimension. Following the classical approach of [36], suppose cells move with velocity $\pm v$ and switch direction with rates

$$\lambda^{\pm} = \lambda_0 \mp \beta \partial_x c,$$

where $c(x,t)$ is the chemoattractant concentration and $\beta > 0$ measures sensitivity to gradients. Passing to the diffusion limit yields

$$\partial_t p = D\partial_{xx} p - \chi \partial_x (p \partial_x c),$$

where D is the effective diffusion coefficient and χ is the chemotactic sensitivity. In higher dimensions this becomes

$$\partial_t p = D\Delta p - \chi \nabla \cdot (p \nabla c).$$

This derivation assumes that directional bias is weak at the microscopic scale but accumulates macroscopically

to produce drift along chemical gradients. More refined velocity-jump and kinetic descriptions are discussed in [37, 38].

5.2 Nondimensionalization of the Keller–Segel Model

Consider the classical Keller–Segel system

$$\begin{cases} n_t = D_n \Delta n - \chi \nabla \cdot (n \nabla c), \\ c_t = D_c \Delta c + \alpha n - \beta c. \end{cases}$$

Introduce characteristic scales

$$n = N\tilde{n}, \quad c = C\tilde{c}, \quad x = L\tilde{x}, \quad t = \frac{L^2}{D_c}\tilde{t}.$$

Substituting into the system and omitting tildes gives

$$\begin{cases} n_t = \delta \Delta n - \chi^* \nabla \cdot (n \nabla c), \\ c_t = \Delta c + \sigma n - \kappa c, \end{cases}$$

where

$$\delta = \frac{D_n}{D_c}, \quad \chi^* = \frac{\chi C}{D_c}, \quad \sigma = \frac{\alpha N L^2}{D_c}, \quad \kappa = \frac{\beta L^2}{D_c}.$$

The parameter δ measures the relative strength of cellular diffusion to chemical diffusion, while χ^* quantifies chemotactic sensitivity. The parameter σ represents chemical production relative to diffusion, and κ characterizes chemical decay.

The nondimensional form clarifies important dynamical regimes. Large χ^* and σ promote aggregation, whereas large δ and κ stabilize the system through diffusion and chemical decay. In many biological settings $D_c \gg D_n$, so $\delta \ll 1$.

5.3 One-Dimensional Keller–Segel Model with Logistic Growth

We consider

$$\begin{aligned} \partial_t n &= D_n \partial_{xx} n - \chi \partial_x (n \partial_x c) + rn\left(1 - \frac{n}{K}\right), \\ \partial_t c &= D_c \partial_{xx} c + \alpha n - \beta c, \end{aligned} \tag{7}$$

for $x \in (0, L)$ and $t > 0$, subject to homogeneous Neumann boundary conditions

$$\partial_x n = \partial_x c = 0 \qquad \text{on } x = 0, L, \tag{8}$$

and nonnegative initial data.

5.3.1 Existence and Global Boundedness

Theorem 5.1 (Local existence). *Let $n_0, c_0 \in H^1(0, L)$ with $n_0, c_0 \geq 0$. Then there exists $T > 0$ such that system (7)–(8) admits a unique classical solution*

$$n, c \in C([0, T]; H^1(0, L)).$$

Moreover,

$$n(x, t) \geq 0, \qquad c(x, t) \geq 0.$$

Proof. The diffusion operators with Neumann boundary conditions generate analytic semigroups on $L^2(0, L)$. Writing the system in mild form,

$$\begin{aligned} n(t) &= e^{tA_n} n_0 + \int_0^t e^{(t-s)A_n} F_1(n, c)\, ds, \\ c(t) &= e^{tA_c} c_0 + \int_0^t e^{(t-s)A_c} F_2(n, c)\, ds, \end{aligned}$$

where

$$\begin{aligned} F_1(n, c) &= -\chi \partial_x (n \partial_x c) + rn\left(1 - \frac{n}{K}\right), \\ F_2(n, c) &= \alpha n - \beta c, \end{aligned}$$

standard semigroup estimates and the embedding

$$H^1(0, L) \hookrightarrow L^\infty(0, L)$$

show that the nonlinearities are locally Lipschitz in $H^1(0, L)$. A Banach fixed-point argument therefore yields a unique local classical solution. Positivity follows from the parabolic maximum principle. □

Theorem 5.2 (Global existence and boundedness). *The local solution extends globally in time. Moreover, there exist constants $M_n, M_c > 0$ such that*

$$0 \leq n(x, t) \leq M_n, \qquad 0 \leq c(x, t) \leq M_c$$

for all $t > 0$.

Proof. Integrating the first equation gives

$$\frac{d}{dt} \int_0^L n\, dx = r \int_0^L n\left(1 - \frac{n}{K}\right) dx,$$

which yields a uniform L^1 bound for n. Multiplying the equations by n and c, respectively, and integrating by parts lead to

$$\frac{d}{dt} \|n\|_{L^2}^2 + D_n \|\partial_x n\|_{L^2}^2 \leq C\|n\|_{L^2}^2 \|c\|_{H^2}^2 + C\|n\|_{L^2}^2,$$

and

$$\frac{d}{dt} \|c\|_{L^2}^2 + D_c \|\partial_x c\|_{L^2}^2 + \beta \|c\|_{L^2}^2 \leq C\|n\|_{L^2}^2.$$

Parabolic regularity implies

$$\|c\|_{H^2} \le C(\|n\|_{L^2} + \|c\|_{L^2}),$$

and Grönwall's inequality yields uniform bounds on finite time intervals. Standard continuation arguments therefore imply global existence.

Positivity follows from the maximum principle. The logistic term prevents unbounded growth of n, while the comparison principle applied to the c-equation gives

$$\|c(t)\|_{L^\infty} \le \max\left\{\|c_0\|_{L^\infty}, \frac{\alpha K}{\beta}\right\}.$$

□

5.3.2 Steady States and Linear Stability

The homogeneous steady state of (7) is

$$(n_s, c_s) = \left(K, \frac{\alpha K}{\beta}\right).$$

Linearizing about (n_s, c_s) and seeking normal mode solutions

$$(\tilde{n}, \tilde{c}) = (A, B)e^{\lambda t}\cos\left(\frac{m\pi x}{L}\right)$$

gives the eigenvalue problem

$$\lambda \begin{pmatrix} A \\ B \end{pmatrix} = J(\mu_m) \begin{pmatrix} A \\ B \end{pmatrix},$$

where

$$\mu_m = \left(\frac{m\pi}{L}\right)^2,$$

and

$$J(\mu_m) = \begin{pmatrix} -D_n\mu_m - r & \chi K \mu_m \\ \alpha & -D_c\mu_m - \beta \end{pmatrix}.$$

Theorem 5.3 (Turing instability). *The homogeneous steady state is linearly unstable if there exists $m \ge 1$ such that*

$$\alpha\chi K\mu_m > (D_n\mu_m + r)(D_c\mu_m + \beta).$$

Proof. The eigenvalues satisfy

$$\lambda^2 - \operatorname{tr}(J)\lambda + \det(J) = 0.$$

Since the trace is negative, instability occurs precisely when

$$\det(J(\mu_m)) < 0,$$

which yields the stated condition. □

The instability criterion reflects the competition between chemotactic aggregation and stabilizing effects such as diffusion, chemical decay, and logistic damping. Large chemotactic sensitivity χ and production rate α promote pattern formation, whereas diffusion suppresses it.

5.3.3 Lyapunov Stability

To study nonlinear stability near equilibrium, define

$$u = n - K, \qquad v = c - c_s,$$

and consider the Lyapunov functional

$$\mathcal{L}(t) = \frac{1}{2}\int_0^L u^2\,dx + \frac{\gamma}{2}\int_0^L v^2\,dx,$$

with $\gamma > 0$.

Differentiating along solutions and integrating by parts gives

$$\frac{d}{dt}\mathcal{L} \le -\frac{D_n}{2}\|\partial_x u\|_{L^2}^2 - \left(\gamma D_c - \frac{\chi^2 K^2}{D_n}\right)\|\partial_x v\|_{L^2}^2 - \frac{r}{2}\|u\|_{L^2}^2 - (\gamma\beta - C)\|v\|_{L^2}^2.$$

Theorem 5.4 (Nonlinear stability). *Assume*

$$\gamma D_c > \frac{\chi^2 K^2}{D_n},$$

and let the initial data be sufficiently close to (K, c_s) in $H^1(0, L)$. Then

$$\|n(\cdot,t) - K\|_{L^2(0,L)} + \|c(\cdot,t) - c_s\|_{L^2(0,L)} \to 0 \qquad \text{as } t \to \infty.$$

Proof. Under the stated condition, all terms in the Lyapunov estimate are negative definite. Hence there exists $\delta > 0$ such that

$$\frac{d}{dt}\mathcal{L}(t) \le -\delta\mathcal{L}(t).$$

Grönwall's inequality then yields exponential decay:

$$\mathcal{L}(t) \le \mathcal{L}(0)e^{-\delta t}.$$

The conclusion follows immediately. □

The result shows that logistic damping can stabilize the Keller–Segel dynamics when chemotactic effects are sufficiently weak.

5.4 Numerical Methods, Computational Challenges, and Validation

Analytical solutions for nonlinear chemotaxis–reaction systems are generally unavailable except in highly simplified settings, making numerical simulation indispensable for studying aggregation dynamics, traveling bands, instability growth, and long-time pattern formation. Numerical schemes for Keller–Segel-type systems must simultaneously address several competing requirements, including stability near steep gradients, positivity preservation, accurate chemotactic flux approximation, mass balance, and computational efficiency in multidimensional settings. Modern numerical investigations therefore combine classical discretization techniques with adaptive stabilization, structure-preserving formulations, multiscale coupling, and data-driven parameter inference [4, 16, 21, 33].

Classical finite difference methods remain widely used because of their simplicity and low computational cost, particularly for structured domains and benchmark studies. Finite element methods are advantageous for irregular geometries and heterogeneous biological environments, while adaptive mesh refinement techniques provide improved resolution near aggregation peaks and blow-up regions. Hybrid particle–continuum approaches are especially useful when macroscopic density evolution interacts with discrete cellular behavior. More recently, pseudo-spectral and exponential integrator methods have become attractive for resolving smooth chemotactic structures with high spatial accuracy.

Compared with standard finite difference discretizations, finite element schemes generally provide superior geometric flexibility and variational consistency, especially in heterogeneous tissue domains. However, they often require more sophisticated solvers and stabilization procedures for strongly advective chemotactic fluxes. Spectral methods exhibit exponential spatial convergence for smooth periodic solutions and outperform low-order schemes in resolving long-range spatial correlations, although Gibbs oscillations and aliasing errors may become significant near steep fronts or near-singular aggregation events. Adaptive finite volume and positivity-preserving flux-limited schemes are more robust in high-gradient regimes and better maintain non-negativity, but at increased computational complexity. Consequently, no single numerical framework is universally optimal for all chemotaxis systems. Explicit finite difference methods remain useful for mechanistic interpretation and benchmark validation, whereas structure-preserving implicit or adaptive schemes are preferable for stiff multiscale simulations and near blow-up regimes.

To illustrate the numerical formulation concretely, we consider finite difference discretizations of the Keller–Segel system with logistic growth:

$$\begin{aligned} \partial_t n &= D_n n_{xx} - \chi (n c_x)_x + r n (1 - n/K), \\ \partial_t c &= D_c c_{xx} + \alpha n - \beta c, \end{aligned} \tag{9}$$

defined on the interval $x \in [0, L]$ with no-flux boundary conditions

$$n_x(0) = n_x(L) = c_x(0) = c_x(L) = 0.$$

5.4.1 *Finite Difference Scheme for 1D Chemotaxis*

The spatial domain is partitioned into I subintervals of width $\Delta x = L/I$, and n_i^k approximates $n(x_i, t^k)$ at grid points $x_i = i\Delta x$ and times $t^k = k\Delta t$. Using a forward Euler discretization in time, the diffusion term is approximated by

$$(n_{xx})_i^k \approx \frac{n_{i+1}^k - 2n_i^k + n_{i-1}^k}{(\Delta x)^2}.$$

The chemotactic flux is written as

$$F = -\chi n c_x.$$

Using midpoint averaging and central differences,

$$F_{i+\frac{1}{2}}^k = -\chi n_{i+\frac{1}{2}}^k \frac{c_{i+1}^k - c_i^k}{\Delta x}, \qquad n_{i+\frac{1}{2}}^k = \frac{1}{2}(n_i^k + n_{i+1}^k),$$

with analogous expressions for $F_{i-\frac{1}{2}}^k$. The chemotactic divergence becomes

$$((n c_x)_x)_i^k \approx \frac{F_{i+\frac{1}{2}}^k - F_{i-\frac{1}{2}}^k}{\Delta x}.$$

The resulting update equation for the cell density is

$$n_i^{k+1} = n_i^k + \Delta t \left[D_n \frac{n_{i+1}^k - 2n_i^k + n_{i-1}^k}{(\Delta x)^2} - \frac{F_{i+\frac{1}{2}}^k - F_{i-\frac{1}{2}}^k}{\Delta x} + r n_i^k \left(1 - \frac{n_i^k}{K}\right) \right].$$

Similarly, the chemoattractant concentration satisfies

$$c_i^{k+1} = c_i^k + \Delta t \left[D_c \frac{c_{i+1}^k - 2c_i^k + c_{i-1}^k}{(\Delta x)^2} + \alpha n_i^k - \beta c_i^k \right].$$

The no-flux conditions are implemented through mirror values,

$$n_{-1} = n_1, \qquad n_{I+1} = n_{I-1},$$

and similarly for c. The explicit formulation is computationally inexpensive and straightforward to implement, although stability constraints impose

$$\Delta t \leq \frac{(\Delta x)^2}{2D_n}$$

for the diffusion term. Chemotactic advection introduces additional restrictions, particularly when steep gradients emerge. Central differencing may generate oscillations near aggregation fronts, whereas upwind or flux-limited formulations improve robustness in strongly advective regimes.

5.4.2 *Finite Difference Scheme for 2D Chemotaxis*

For two-dimensional simulations, we discretize the domain using uniform spacing $\Delta x = \Delta y = h$ and denote the numerical approximations by $n_{i,j}^k$ and $c_{i,j}^k$.

The cell density equation becomes

$$\begin{aligned} n_{i,j}^{k+1} = n_{i,j}^k + \Delta t \Bigg[& D_n \left(\frac{n_{i+1,j}^k - 2n_{i,j}^k + n_{i-1,j}^k}{h^2} \right. \\ & \left. + \frac{n_{i,j+1}^k - 2n_{i,j}^k + n_{i,j-1}^k}{h^2} \right) \\ & - \frac{F_{i+\frac{1}{2},j}^{x,k} - F_{i-\frac{1}{2},j}^{x,k}}{h} \\ & - \frac{F_{i,j+\frac{1}{2}}^{y,k} - F_{i,j-\frac{1}{2}}^{y,k}}{h} \\ & + r n_{i,j}^k \left(1 - \frac{n_{i,j}^k}{K} \right) \Bigg], \end{aligned}$$

where

$$\begin{aligned} F_{i+\frac{1}{2},j}^{x,k} &= \frac{1}{2}(n_{i+1,j}^k + n_{i,j}^k)\frac{c_{i+1,j}^k - c_{i,j}^k}{h}, \\ F_{i,j+\frac{1}{2}}^{y,k} &= \frac{1}{2}(n_{i,j+1}^k + n_{i,j}^k)\frac{c_{i,j+1}^k - c_{i,j}^k}{h}. \end{aligned}$$

The chemoattractant equation is discretized as

$$\begin{aligned} c_{i,j}^{k+1} = c_{i,j}^k + \Delta t \Bigg[& D_c \left(\frac{c_{i+1,j}^k - 2c_{i,j}^k + c_{i-1,j}^k}{h^2} \right. \\ & \left. + \frac{c_{i,j+1}^k - 2c_{i,j}^k + c_{i,j-1}^k}{h^2} \right) \\ & + \alpha n_{i,j}^k - \beta c_{i,j}^k \Bigg]. \end{aligned}$$

The variables $n(x, y, t)$ and $c(x, y, t)$ denote the densities of motile cells and chemoattractant concentration, respectively. Simulations were performed using

$$\begin{aligned} & D_n = 0.00416, \quad D_c = 0.001, \quad \chi = 1.0, \quad \alpha = 0.005, \\ & \beta = 0.001, \quad r = 2.0, \quad K = 2.0, \end{aligned}$$

with randomized perturbation initial data

$$n = 0.05 + 0.01 \cdot \mathrm{rand}(N+1, N+1),$$

$$c = 0.05 + 0.01 \cdot \mathrm{rand}(N+1, N+1).$$

At early times ($t = 2$, as seen in Figure 1), weak aggregation structures emerge as small spatial inhomogeneities driven by chemotactic signaling. At later times ($t = 10$) as displayed in Figure 2, the system develops pronounced spatiotemporal oscillations and rapidly evolving high-density regions, consistent with nonlinear competition between diffusion, chemotactic attraction, and logistic damping [39, 40]. These simulations demonstrate that chemotaxis alone can generate complex self-organized spatial structures resembling microbial colony aggregation and invasive biological fronts.

Importantly, not all observed numerical patterns are equally robust with respect to parameter variations. The onset of aggregation is relatively insensitive to small perturbations in the initial conditions and persists over a broad range of diffusion and growth parameters. In contrast, strongly chaotic oscillatory states depend sensitively on the chemotactic sensitivity χ, the growth coefficient r, and the chemoattractant production rate α. Increasing χ generally amplifies aggregation intensity and accelerates instability formation, while larger diffusion coefficients suppress fine-scale structures and promote homogenization. Similarly, high logistic damping stabilizes the dynamics and prevents near-singular concentration peaks. Consequently, localized spot patterns and weak aggregation bands are comparatively robust structures, whereas highly irregular chaotic regimes arise only within restricted parameter intervals associated with strong chemotactic forcing and weak diffusion.

5.4.3 *Spectral Discretization of the Keller–Segel Model*

Spectral methods provide substantially higher spatial accuracy for smooth chemotactic solutions and are particularly effective for periodic domains. On the periodic square domain $\Omega = [0, L]^2$, we expand the

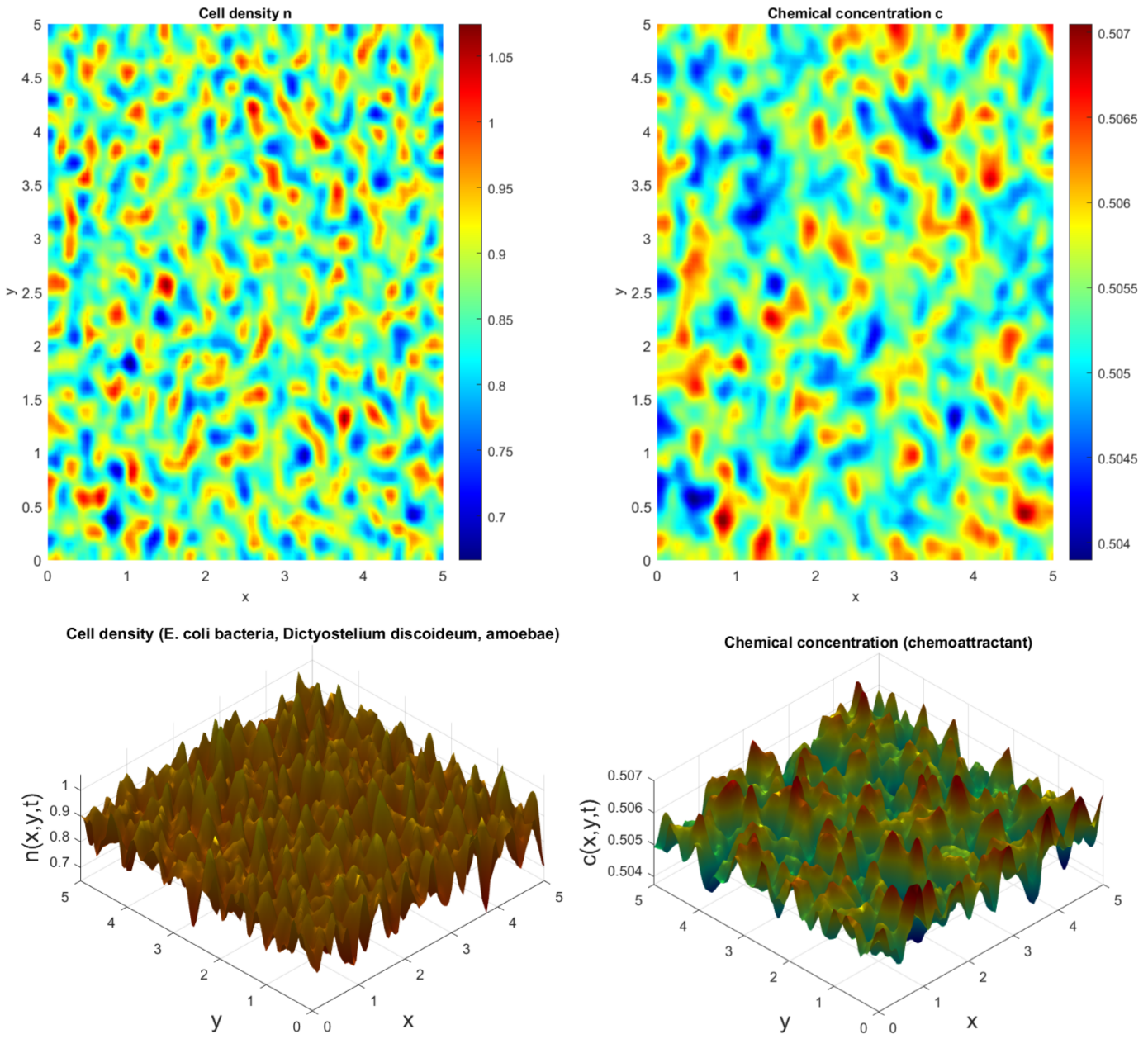

Figure 1. Time evolution of the 2D Keller–Segel model showing chaotic oscillatory patterns in cell density $n(x, y, t)$ at $t = 2$ and $r = 1.0$. The patterns illustrate chemotactic aggregation and spatiotemporal chaos driven by the coupling between n and c.

solution in truncated Fourier series:

$$n(x,y,t) = \sum_{k_x=-N}^{N} \sum_{k_y=-N}^{N} \hat{n}_{k_x,k_y}(t) e^{i(k_x \kappa x + k_y \kappa y)}, \quad (10)$$

$$c(x,y,t) = \sum_{k_x=-N}^{N} \sum_{k_y=-N}^{N} \hat{c}_{k_x,k_y}(t) e^{i(k_x \kappa x + k_y \kappa y)}, \quad (11)$$

where $\kappa = 2\pi/L$.

The Laplacian operator diagonalizes in Fourier space:

$$\widehat{\nabla^2 u} = -\kappa^2 (k_x^2 + k_y^2) \hat{u}_{k_x,k_y}.$$

The nonlinear chemotactic term is evaluated through a pseudo-spectral procedure:

1. Transform $\hat{n}$ and $\hat{c}$ to physical space using inverse FFT.
2. Compute ∇c, evaluate $n\nabla c$, and compute the divergence.
3. Transform the nonlinear contribution back to Fourier space.

Temporal integration is performed using semi-implicit or exponential time-differencing methods such

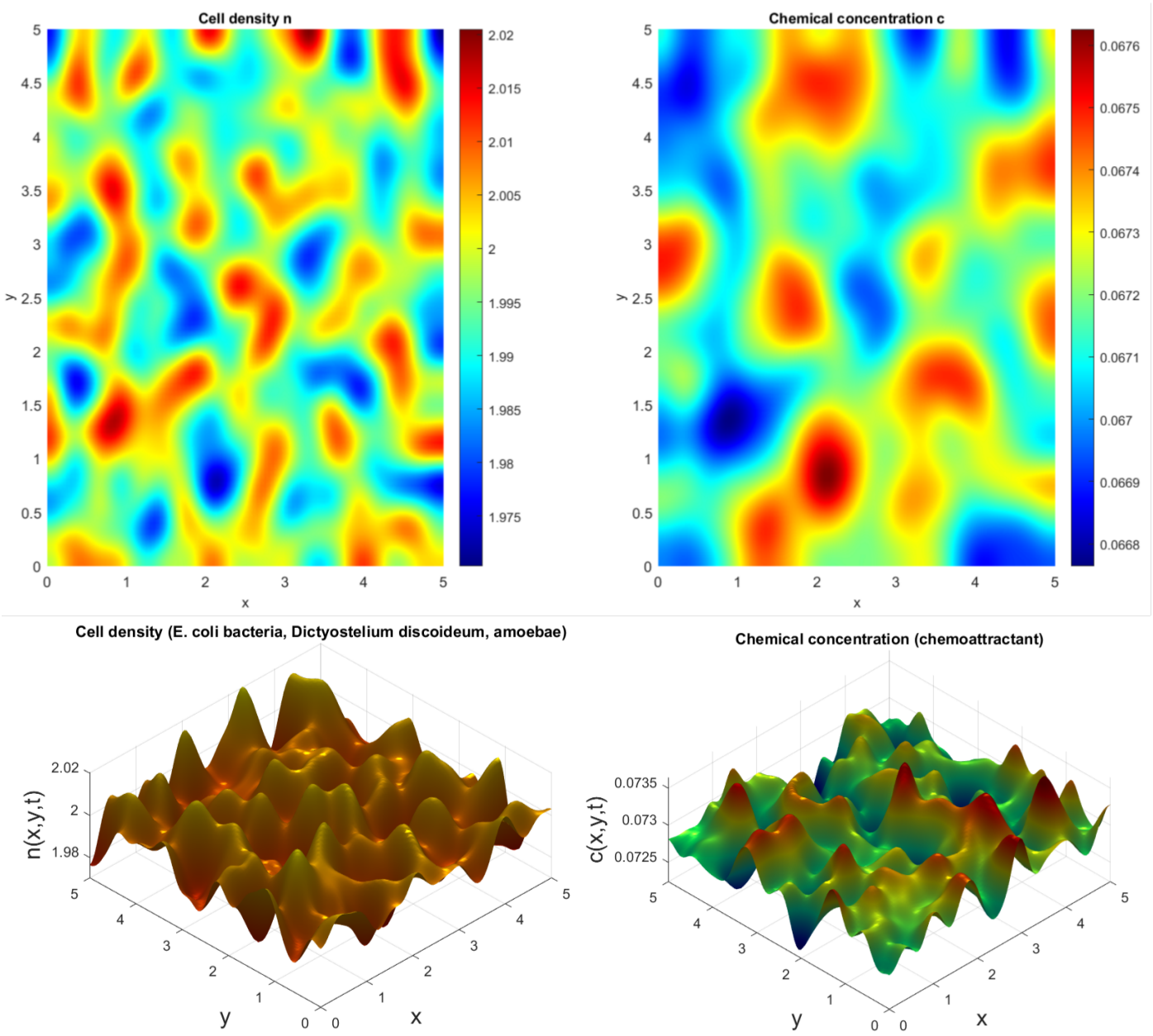

Figure 2. Time evolution of the 2D Keller–Segel model showing chaotic oscillatory patterns in cell density $n(x, y, t)$ at $t = 10$ and $r = 5.0$. The patterns illustrate chemotactic aggregation and spatiotemporal chaos driven by the coupling between n and c.

as ETDRK4 [41, 42]. Compared with explicit finite difference schemes, spectral methods achieve substantially improved spatial accuracy and resolve dominant instability wavelengths more efficiently. However, they are less robust near steep fronts and require dealiasing procedures, such as the $2/3$ truncation rule, to suppress spurious mode interactions.

5.4.4 Positivity Preservation and Mass Balance

Maintaining non-negativity of n and c is essential for biological consistency. Explicit central-difference discretizations preserve positivity only under sufficiently restrictive time-step conditions. Diffusion terms satisfy a discrete maximum principle provided

$$\Delta t \leq \frac{1}{2d} \frac{(\Delta x)^2}{D},$$

while chemotactic fluxes may still generate oscillatory undershoots near sharp gradients. Flux limiters, upwind reconstructions, and positivity-preserving finite volume formulations generally outperform standard central schemes in this respect.

The finite difference discretization preserves discrete mass balance. Summation of the n equation over all grid points yields cancellation of internal diffusion

and chemotactic fluxes, leaving only the logistic source contribution:

$$\sum_i n_i^{k+1} = \sum_i n_i^k + \Delta t \sum_i r n_i^k \left(1 - \frac{n_i^k}{K}\right).$$

When $r = 0$, total cell mass remains conserved to machine precision. Numerical experiments showed relative conservation errors below 10^{-12} over long-time simulations, confirming consistency of the flux discretization.

5.4.5 *Validation and Experimental Consistency*

To assess numerical reliability, several benchmark tests were performed using analytical predictions, convergence studies, and experimentally observed chemotactic behaviors.

Traveling bacterial bands reported in classical chemotaxis experiments [2] were reproduced numerically using localized Gaussian initial conditions. The simulated bands propagated while approximately preserving shape and amplitude, consistent with experimentally observed chemotactic migration dynamics in bacterial populations.

Linear stability theory was also used for validation. The dispersion relation predicts a dominant unstable wavenumber $k_{\max}$ corresponding to a preferred aggregation wavelength

$$\lambda_{\max} = \frac{2\pi}{k_{\max}}.$$

Table 2. Parameter values used for linear stability validation studies.

Parameter	Symbol	Value
Cell diffusivity	D_n	1
Chemoattractant diffusivity	D_c	10
Chemotactic sensitivity	χ	200
Chemoattractant production rate	α	1
Chemoattractant decay rate	β	0
Domain size	$L_x \times L_y$	50×50
Boundary conditions	–	Periodic

Using the parameter set in Table 2, the simulated dominant wavelength agreed closely with theoretical predictions obtained from Fourier analysis of the numerical patterns. This comparison is demonstrated in Table 3.

The numerical patterns also exhibit qualitative agreement with experimentally observed aggregation phenomena in bacterial colonies and amoeboid chemotaxis studies, particularly regarding spot merging, traveling bands, and dynamically evolving cluster structures. Although exact biological parameter estimation remains difficult because many coefficients vary across species and environmental conditions, recent developments in inverse modeling and machine-learning-assisted parameter inference have improved calibration of chemotaxis models against imaging and tracking data [21, 33]. Parameters such as diffusivities, chemotactic sensitivity, and production rates are commonly estimated from fluorescence imaging, cell tracking experiments, and migration assays. Nevertheless, parameter uncertainty remains a significant limitation in predictive biological simulations.

In Table 4, we further validate numerical accuracy, a convergence study was conducted by successive mesh refinement. Reducing the mesh spacing by a factor of two and scaling the time step accordingly produced approximately fourfold reductions in the L^2 error norm, confirming the expected second-order spatial accuracy of the central difference discretization.

Table 5 summarizes the main computational characteristics of several numerical approaches commonly used for Keller–Segel-type chemotaxis systems. Explicit finite difference schemes remain attractive because of their simplicity and low computational cost, although their stability restrictions become severe near steep aggregation fronts. Finite element methods provide greater geometric flexibility and variational consistency, particularly in heterogeneous domains, but often require additional stabilization procedures for strongly advective chemotactic fluxes. Spectral methods achieve very high spatial accuracy for smooth periodic solutions

Table 3. Comparison between theoretical predictions and numerical measurements of dominant aggregation wavelengths.

Case	Theoretical $\lambda_{\max}$	Numerical $\lambda_{\max}$	Relative Error
Weak chemotaxis	12.4	12.8	3.2%
Moderate chemotaxis	8.7	8.5	2.3%
Strong chemotaxis	5.9	6.1	3.4%

Table 4. Convergence study for the finite difference discretization.

Grid Size	Time Step Δt	L^2 Error	Convergence Rate
50×50	1.0×10^{-3}	–	–
100×100	2.5×10^{-4}	3.12×10^{-2}	–
200×200	6.25×10^{-5}	7.98×10^{-3}	1.97

Table 5. Comparison of numerical methods for chemotaxis and reaction–diffusion models.

Method	**Strengths**	**Limitations**	**Typical Applications**
Finite Difference Methods (FDM)	Simple implementation; efficient for structured grids; easy to analyze stability	Limited flexibility for complex geometries; may suffer from numerical diffusion	Classical Keller–Segel models; benchmark simulations
Finite Element Methods (FEM)	High geometric flexibility; strong theoretical foundation; good accuracy	Higher computational cost; complex implementation; requires mesh generation	Irregular domains; coupled chemotaxis–fluid systems
Spectral Methods	Very high accuracy for smooth solutions; exponential convergence; efficient for periodic/simple domains	Poor performance for discontinuities or sharp fronts; less flexible for complex geometries	Smooth chemotaxis solutions; pattern formation; benchmark PDE solvers
Adaptive Mesh Refinement (AMR)	Efficient resolution of steep gradients and blow-up regions; adaptive accuracy	Algorithmic complexity; overhead in mesh adaptation; harder parallelization	Blow-up analysis; localized aggregation phenomena
Hybrid Particle-Based Methods	Captures individual-level dynamics; good for multiscale coupling	Computationally expensive for large populations; statistical noise	Agent-based chemotaxis; hybrid continuum–discrete models

through exponential convergence, yet may suffer from aliasing errors and reduced robustness near discontinuities. Positivity-preserving finite volume schemes are especially effective in maintaining biologically meaningful nonnegative densities during strong aggregation, while adaptive mesh refinement techniques improve local resolution near singular structures and evolving peaks at the expense of higher computational complexity. Overall, the comparison illustrates the trade-off between numerical accuracy, stability, robustness, and computational efficiency in modern chemotaxis simulations [4, 21, 43, 44].

Overall, the validation studies confirm that the numerical framework accurately reproduces traveling bands, instability-driven aggregation, dominant wavelength selection, and long-time pattern evolution. At the same time, the comparison with alternative numerical approaches highlights the trade-off between simplicity, robustness, stability, and computational efficiency that characterizes modern numerical simulation of chemotaxis–reaction systems.

6 Applications in Microbial Ecology

We now turn to explicit applications of chemotaxis–reaction models to phenomena observed in microbial ecology. By comparing model outcomes with experimental data, we can assess the validity of these models and refine them to better capture biological reality. Below we discuss several key application domains, illustrating how the mathematical frameworks described above have enhanced our understanding of microbial behaviors.

6.1 Bacterial Aggregation and Pattern Formation

One of the most striking consequences of chemotaxis is the formation of spatial patterns in bacterial colonies. Classic experiments by [23, 35] demonstrated that certain strains of *E. coli* can self-organize into arrays of high-density spots, concentric rings, and traveling waves when grown on semisolid agar containing attractant and nutrients. These patterns arise from chemotaxis in combination with growth and substrate depletion. Mathematical models have been able to

reproduce many features of these patterns, lending credence to the idea that they result from chemotactic instabilities.

For example, consider a simple model for a bacterial colony expanding on a plate: bacteria consume a nutrient (serving as a chemoattractant) and move chemotactically toward it. A representative model might be:

$$\begin{aligned} \partial_t n &= D\Delta n - \chi \nabla \cdot (n \nabla c) + \mu n \frac{c}{c + K_s}, \\ \partial_t c &= D_c \Delta c - \kappa n \frac{c}{c + K_s}, \end{aligned} \tag{12}$$

where $n(x,t)$ is bacterial density and $c(x,t)$ nutrient concentration. Initially, nutrient is abundant and bacteria are mostly near the inoculation point. As they proliferate and consume nutrient, a nutrient gradient develops outward, drawing bacteria into an expanding ring. The above model can produce a moving band of bacteria followed by a depleted region (a trailing void of nutrient), qualitatively matching observations of concentric ring patterns (often called "bull's-eye" patterns) [23]. The equations capture how the outermost cells always find fresh nutrient ahead and move outward, while behind them nutrient is depleted and cells may starve or slow down, creating a ring-like high-density frontier.

More intricate patterns like spotted arrays require additional ingredients. Budrene and Berg observed spots forming in certain conditions and proposed that an attractant produced by bacteria (e.g. a metabolic byproduct like a specific amino acid) might be causing aggregation. This led to models with self-secreted attractants (similar to the K-S model structure). Reaction terms such as cell mortality or dormancy at high density were introduced to explain why aggregates eventually stabilize or stop growing (preventing blow-up in real life). For instance, including a finite carrying capacity (logistic limit) or a toxin produced at high density can yield stable aggregates of finite cell population, corresponding to the observed spots.

Models have been compared to experiments by measuring pattern metrics: number of spots vs initial cell density, spacing between aggregates vs parameters, speed of outward moving rings, etc. Many qualitative and semi-quantitative agreements have been found [45]. Notably, models predict that the chemotactic sensitivity and nutrient uptake rates control whether patterns are diffuse or sharply separated. With high chemotactic sensitivity, cells cluster tightly (spots); with lower sensitivity, they form more graded patterns or no pattern at all (uniform spread). These trends have been confirmed by manipulating bacterial mutants with different chemotactic prowess or using different chemoeffector chemicals.

Another context of bacterial pattern formation is swarming motility on surfaces, as in *Bacillus subtilis*. Swarming colonies often exhibit branched or dendritic patterns. While those are partly due to growth and nutrient diffusion, some studies suggest chemotaxis toward nutrients or self-generated surfactants guides the branching. PDE models combining chemotaxis with reaction–diffusion of surfactant have been proposed to replicate branching patterns seen in *Bacillus* and other motile bacteria, achieving a qualitative resemblance to the gorgeous fractal-like colony morphologies observed in experiments [46]. Chemotaxis in these models biases movement at the colony edge, amplifying slight protrusions into full-fledged branches.

In summary, chemotaxis–reaction models have become an indispensable tool to interpret bacterial pattern formation. They provide a mechanistic explanation: patterns emerge as an outcome of cells moving up chemical gradients that they themselves modify through consumption or secretion, coupled with growth and competition. This reinforces the concept that complex colony patterns need not require an elaborate genetic program or cell–cell communication scheme; they can be self-organized through simple rules of movement and feeding, as captured by these mathematical models.

6.2 Biofilm Growth and Spatial Structuring

Biofilms are communities of microorganisms that stick to each other and to surfaces, encased in a self-produced matrix. They exhibit intricate internal spatial organization, with gradients of nutrients, oxygen, and signaling molecules across the biofilm depth. Chemotaxis can influence biofilm development in the initial colonization phase and possibly within the biofilm structure itself.

During *biofilm initiation*, motile bacteria in the surrounding fluid may be attracted to chemical cues on a surface. For example, a surface might be coated with nutrients or a conditioning film that diffuses into the fluid, creating a gradient that planktonic cells sense. Alternatively, pioneer bacteria that randomly attached could start secreting an attractant (or a quorum sensing signal) that draws more swimmers to join them.

Models of this process use chemotaxis equations in a fluid (sometimes coupling with flow if in a channel) to estimate the rate of surface colonization. Such models show that chemotaxis can dramatically increase the rate at which a biofilm seed forms compared to purely random attachment, especially under flow conditions where otherwise cells would be swept away [47]. By aligning with flow and moving toward the surface via chemotaxis, bacteria effectively filter themselves out of the fluid to the surface.

Within established biofilms, bacteria are often embedded in a dense matrix and may lose flagellar motility, so chemotaxis in the classical sense might stop. However, some biofilms have peripheral zones of active movement or channels where cells swim. Chemotaxis within a biofilm could lead to microstructure formation, such as voids or channels: if attractant is higher in some regions (e.g. near nutrient source at biofilm top), cells might migrate that way, leaving behind low-density pockets. Moreover, gradients of signaling molecules (quorum sensing signals, or oxygen) can cause differential gene expression in layers of the biofilm, which might not be movement per se but can be modeled similarly to chemotactic response in terms of patterns of active/inactive cells.

Mathematical models for biofilms often extend chemotaxis–reaction models by adding an equation for the *extracellular polymeric substance* (EPS) matrix that cells produce. A typical biofilm model might have three components: cells $n(\mathbf{x}, t)$, a public good or signal $c(\mathbf{x}, t)$, and matrix density $m(\mathbf{x}, t)$. Equations could be:

$$\begin{aligned} \partial_t n &= D_n \Delta n - \chi \nabla \cdot (n \nabla c) + \alpha(c)\, n - \delta(m)\, n, \\ \partial_t c &= D_c \Delta c + f(n, c), \\ \partial_t m &= D_m \Delta m + \eta n - \lambda m. \end{aligned} \tag{13}$$

Here $\alpha(c)$ might model growth of cells depending on nutrient c (or activation of cells by a signal c), and $\delta(m)$ might represent a detachment or reduced viability rate that increases with matrix m (cells deep in matrix may starve or suffocate). The matrix m is produced by cells at rate η and decays or disperses at rate λ. In such a model, chemotaxis ($-\chi \nabla \cdot (n \nabla c)$) could cause the cells to cluster in regions of higher nutrient (often near the biofilm surface), yielding layered structures: a dense active layer on the outside and an inner core of mostly inert cells. This aligns with experimental observations of many biofilms, which have metabolically active peripheries and inactive cores due to nutrient gradients.

The interplay of chemotaxis and matrix production can also generate fingering patterns of biofilm spread. If cells move toward nutrients at the edges, they might cause the biofilm front to become unstable and form finger-like protrusions, similar to diffusion-limited growth patterns. Models including chemotaxis have shown more pronounced fingering compared to models without chemotaxis, suggesting that directed movement contributes to the heterogeneous expansion of biofilm fronts.

Quorum sensing (QS) is another factor. Some biofilm models incorporate QS signaling, which often induces matrix production above a threshold. Chemotaxis toward QS signals (autoinducers) has been reported in a few species (e.g. *Pseudomonas aeruginosa* is attracted to certain QS molecules it produces). This creates a positive feedback: more cells $\rightarrow$ more QS $\rightarrow$ cells aggregate more. It's reminiscent of Keller–Segel with c as the autoinducer. Including this can lead to rapid collapse of cells into a biofilm once a threshold population is present, offering a mechanism for the often observed sudden maturation of biofilms after a lag phase.

In summary, chemotaxis–reaction models give insight into how motile bacteria transition to a biofilm lifestyle and how spatial heterogeneities within biofilms might be established. They emphasize that even in the largely sessile context of biofilms, the initial and peripheral movement guided by chemical gradients can dictate the ultimate architecture of these microbial cities.

6.3 Microbial Competition and Coexistence

In natural ecosystems, multiple microbial species often coexist and compete for resources. Spatial structure mediated by chemotaxis can be a key determinant of which species dominate and whether competitors can stably coexist. Mathematical models with multiple species and chemotaxis (as discussed in Section 3.2) have been used to explore scenarios like competition for a single nutrient, predator–prey interactions, and mutualistic relationships.

One simple scenario is two bacterial species, A and B, both feeding on and attracted to a common nutrient. In a well-mixed (zero-dimensional) Lotka–Volterra competition model, one species would typically exclude the other unless their competition is perfectly balanced. However, if we allow space and chemotaxis, the outcome can be different. For instance, species A might be a faster consumer of nutrient but less motile, whereas species B is highly motile (strong chemotaxis)

but not as efficient at growth. A PDE model may show that A saturates the area near the nutrient source, but B forms a ring further out, intercepting nutrient diffusing outward. The spatial segregation allows B to survive on the "leftover" nutrient that escapes A's immediate vicinity. Coexistence can thus emerge from a spatial partitioning of the habitat. Budrene and Berg [35] had demonstrated such effects in a model and related it to observed patterns in some microbial communities. Analytically, one finds conditions (like relative values of $\chi_1, \chi_2, D_1, D_2, r_1, r_2$) that permit non-uniform steady states where $n_1(\mathbf{x})$ and $n_2(\mathbf{x})$ are both nonzero in disjoint regions. These correspond to coexistence states. Stability analysis can then identify if those coexistence states are robust or if one species will eventually displace the other.

Another interesting case is attraction–repulsion interactions. Suppose species A produces a chemical that species B finds repellent (perhaps a toxin), and B produces an attractant that A seeks (maybe A preys on B). This creates a chase-and-escape dynamic: A chases B chemotactically (attracted by B's signal or presence), while B runs away (chemically avoiding A or the toxin A makes). Depending on parameters, several outcomes are possible: one species might corner and eliminate the other, or they may reach a dynamic equilibrium with B congregating in regions where the toxin from A accumulates less, and A patrolling around those regions. PDE models of this nature (also known as pursuit–evasion models) can exhibit rich patterns like rotating spirals of predators and prey, or stable spatial oscillations. While originally studied in macro-scale predator–prey context, analogous behavior could occur in microbes, for example, bacteriophages (viruses) chasing bacteria that move, or two bacterial strains where one emits a phage or bacteriologic. Tao and Winkler [48] used a chemotactic pursuit–evasion model to illustrate such spatiotemporal patterns and suggested experiments to observe them in engineered E. coli strains.

Mutualistic interactions can also be spatially organized by chemotaxis. If species A produces something beneficial that attracts species B, and B in turn produces another attractant for A (cross-chemotaxis), they could form intermingled patterns or layered structures. For instance, one might see alternating bands of A and B forming a stripe pattern, each moving toward a chemical cue from the other until equilibrium. This is somewhat analogous to Turing patterns but with cross-diffusion (cross-chemotaxis) rather than cross-reaction. The mathematics shows that such cross interactions can broaden the parameter range for pattern formation. In fact, one can derive conditions similar to Turing's for the symmetric two-species chemotaxis system: roughly, if each species strongly responds to the other's signal, symmetry can break and periodic spatial niches form.

From an ecological viewpoint, these models highlight that chemotaxis adds a layer of complexity to classic competition outcomes. Spatial heterogeneity enables diversity: microbes can avoid direct competition by moving, effectively creating their own microniches. Coexistence is often promoted by differential chemotactic abilities (one is better at finding high concentration spots, the other maybe endures low concentration areas). There is also the possibility of *rock-paper-scissors* type cyclic competition in spatial settings, maintained by localized chemotactic chasing and escaping, which has been proposed to explain biodiversity in soil communities.

Experimentally validating these predictions is challenging but some microfluidic experiments allow two strains to compete in a controlled arena with imposed gradients. For example, two *Pseudomonas* strains with different chemotaxis receptors for different nutrients can be placed in a device with multiple nutrient sources. One can observe spatial segregation if each strain specializes in a different nutrient (even if one nutrient is slightly preferred by both). Models accurately predicted which strain would dominate which locale, confirming the role of chemotactic niche partitioning.

6.4 Environmental Systems and Bioremediation

Chemotaxis plays a critical role in environmental microbiology, where microbes encounter patchy resources and pollutants. Models that include chemotaxis are used to understand processes such as bioremediation (bacteria cleaning up contaminants), nutrient cycling in soil, and microbial activity in the ocean.

In bioremediation, certain bacteria can degrade pollutants like hydrocarbons, solvents, or pesticides. Many of these bacteria are chemotactic to the pollutants themselves or to compounds associated with the pollutants. For example, *Pseudomonas putida* is known to move toward toluene, a toxic solvent, which it can then degrade. A chemotaxis–reaction model for this scenario might include bacterial density $n(\mathbf{x}, t)$, pollutant concentration $p(\mathbf{x}, t)$, and perhaps oxygen $o(\mathbf{x}, t)$ (since degradation might be aerobic).

Equations could be:

$$\begin{aligned}\partial_t n &= D_n \Delta n - \chi \nabla \cdot (n \nabla p) + \mu n \frac{p}{p + K_p} \frac{o}{o + K_o}, \\ \partial_t p &= D_p \Delta p - \gamma n \frac{p}{p + K_p}, \\ \partial_t o &= D_o \Delta o - \theta n \frac{o}{o + K_o},\end{aligned} \tag{14}$$

with appropriate initial and boundary conditions (e.g. a spill of pollutant at some location). This model says: bacteria move towards higher pollutant concentration; they grow using pollutant and oxygen (modeled by a double Monod uptake term); the pollutant is consumed and oxygen is consumed in the process. Simulations of such models can inform cleanup strategies: for instance, they can show that bacteria will naturally cluster around pollutant plumes, but if oxygen is limited, the degradation might stall, leading to a donut-shaped pattern of bacteria around an untouched pollutant core (because oxygen is depleted near the core). This suggests the need for oxygenation strategies in bioremediation. Indeed, field engineers often inject air or hydrogen peroxide (as oxygen source) to ensure bacteria can keep degrading the pollutant in the core. Models helped quantify how far oxygen penetrates and where bacteria will concentrate, optimizing the injection rates.

In soils, chemotaxis affects nutrient cycles. Plant roots exude various organic compounds (root exudates) that attract soil bacteria (many of which are beneficial for plant growth). Chemotaxis models have been applied to root-microbe interactions, treating a root as a source of attractant diffusing into the soil. Bacteria swarm toward the root in a chemotactic front, potentially outcompeting pathogens via sheer numbers or by forming a protective biofilm on the root surface. Models combining diffusion of exudates with bacterial chemotaxis and growth can reproduce the formation of dense microbial zones (rhizosphere) around roots [49]. They also indicate how changes in exudate profiles (e.g. a plant under stress releases different compounds) will alter the composition of the attracted community.

In aquatic systems, marine bacteria face extremely dilute and transient nutrient patches (like burst of dissolved organic matter from algal cells or marine snow particles). Chemotaxis enables them to capitalize on these micro-scale patches. Blackburn et al. [50] measured bacterial accumulation around a decaying particle and showed it increased uptake of carbon by orders of magnitude compared to non-motile scenario. Models in that study used chemotaxis equations with spherical symmetry around a particle releasing nutrient. The results matched well with microscale observations: a swarm of bacteria builds up around each particle, forming a "microbial halo". These halos accelerate the particle's decomposition, thus affecting carbon flux to the deep ocean (important for global carbon cycle). A remarkable conclusion was that even low concentrations of attractant, if released in a gradient, suffice to draw bacteria from centimeters away within minutes, illustrating the efficiency of chemotaxis in dilute environments [51].

Chemotaxis can also be detrimental in some cases, such as aiding the spread of pathogens. For example, *Vibrio cholerae* (the cholera bacterium) is chemotactic and uses chemotaxis to reach the intestinal lining and find nutrient-rich niches. Models of infection spread sometimes incorporate chemotactic motility of bacteria combined with fluid flow in intestines. They suggest that disrupting chemotactic pathways (via drugs that jam the chemoreceptors) could reduce the pathogen's ability to colonize the host, a potential therapeutic angle.

In all these environmental examples, chemotaxis–reaction models act as virtual labs where scenarios can be tested: e.g., How will a nutrient pulse be utilized by a community? What if temperature (affecting diffusion) or viscosity (affecting swimming) changes? What if we introduce a chemoattractant decay mechanism (like a dispersant breaking down the signal)? These questions are addressed by modifying terms in the equations and simulating outcomes, thus guiding experimentalists and environmental engineers toward the most impactful variables to monitor or control.

6.5 Split-Step Fourier Method for Chemotaxis Models

The *Split-Step Fourier Method* (SSFM) is a widely used numerical technique for solving partial differential equations (PDEs), especially those involving diffusion, dispersion, and nonlinear interactions [52, 53]. Originally developed for problems in nonlinear optics and quantum mechanics, the SSFM has proven to be highly efficient and accurate for a range of biological pattern formation models, including chemotaxis systems. The method benefits from classical operator splitting techniques and theoretical insights into front propagation and traveling waves [54], which are particularly relevant for capturing sharp chemotactic fronts and migrating bacterial bands.

Chemotaxis refers to the movement of biological cells or organisms in response to chemical gradients. Mathematically, chemotaxis models often take the form of coupled reaction-diffusion systems with nonlinear advection (taxis) terms. A typical chemotaxis-reaction system may involve the dynamics of bacterial density $n(x, y, t)$, pollutant concentration $p(x, y, t)$, and oxygen level $o(x, y, t)$, governed by system of equations (14), where D_n, D_p, D_o are diffusion coefficients, χ is the chemotactic sensitivity, and the remaining terms model consumption and logistic growth.

In SSFM, the time evolution is split into linear (diffusion) and nonlinear (reaction and chemotaxis) parts. For a time step Δt, the update for a field u is typically decomposed as:

1. **Nonlinear step:** Advance u by solving the nonlinear terms in physical space:
$$u^* = u^n + \Delta t \cdot N(u^n),$$
where $N(u)$ represents nonlinear terms (e.g., chemotactic fluxes or reaction kinetics).
2. **Linear step:** Apply the Fourier transform to u^*, evolve the linear (diffusion) part in Fourier space, and inverse transform:
$$\hat{u}^{n+1} = e^{-Dk^2\Delta t} \cdot \hat{u}^*,$$
where $\hat{u}$ is the spatial Fourier transform and $k^2 = k_x^2 + k_y^2 + k_z^2$ in 3D.

This splitting offers several advantages: it enables spectral accuracy in space due to the use of fast Fourier transforms (FFTs), allows for efficient handling of stiff diffusive terms, and easily accommodates periodic boundary conditions, which are common in theoretical biology studies.

Application to Chemotaxis Simulation

In the context of bacterial chemotaxis, the SSFM facilitates high-resolution simulations of emergent spatiotemporal patterns such as aggregation rings, traveling pulses, and isolated clusters. For instance, in our 3D simulation, SSFM was employed to evolve bacterial density and substrate fields over time, revealing the formation of isolated bacterial clusters at later times. The method's efficiency allowed for simulations on large domains (e.g., $100 \times 100 \times 100$) with fine spatial grids while preserving stability and accuracy.

Moreover, the SSFM's structure is particularly well-suited to handle the nonlinear chemotactic flux $\nabla \cdot (n\nabla p)$, which is computed in real space before transforming to Fourier space for diffusion. This hybrid approach ensures robustness and clarity in capturing biologically meaningful structures such as ring waves, cluster formation, and oxygen depletion zones.

The SSFM presents a powerful numerical strategy for studying chemotaxis-reaction models, capable of capturing fine-scale biological patterning with spectral precision. Its adaptability to high-dimensional and multi-species systems makes it a promising tool for modeling microbial ecology and related fields.

To investigate the spatiotemporal dynamics of bacterial bioremediation under chemotaxis and resource limitations, we conducted 1D numerical simulations using the Split-Step Fourier Method (SSFM) for the chemotaxis–reaction model described in equation 14. The domain was set to $[-10, 10]$, discretized into 256 grid points, and simulations were carried out for various end times $T = 3, 6, 9, 12$. The evolution of bacterial density $n(x, t)$, pollutant concentration $p(x, t)$, and oxygen level $o(x, t)$ were visualized in a single frame consisting of four subplots as shown in Figure 3.

6.5.1 *Temporal evolution of the bioremediation front*

At $T = 3$ (top-left subplot): The bacterial Gaussian profile has started to sharpen slightly toward the center due to chemotactic drift. Pollutant and oxygen remain close to initial levels. Little degradation has yet occurred.

At $T = 6$ (top-right subplot): Bacteria become more focused at the pollutant-rich center. The pollutant concentration starts to decrease due to uptake, and a mild oxygen dip emerges, indicating active consumption.

At $T = 9$ (bottom-left subplot): A strong bacterial peak forms, with local depletion of both pollutant and oxygen. The pollutant profile becomes flatter, and the oxygen shows a more prominent central dip.

At $T = 12$ (bottom-right subplot): The central region shows significant degradation, with bacteria still aggregating near residual pollutant zones. Oxygen is heavily depleted at the center, suggesting aerobic degradation has peaked and may be diffusion-limited.

6.5.2 *Biological and physical interpretation*

The simulation reveals several biologically and physically meaningful features:
Chemotactic aggregation: Bacteria sense and migrate

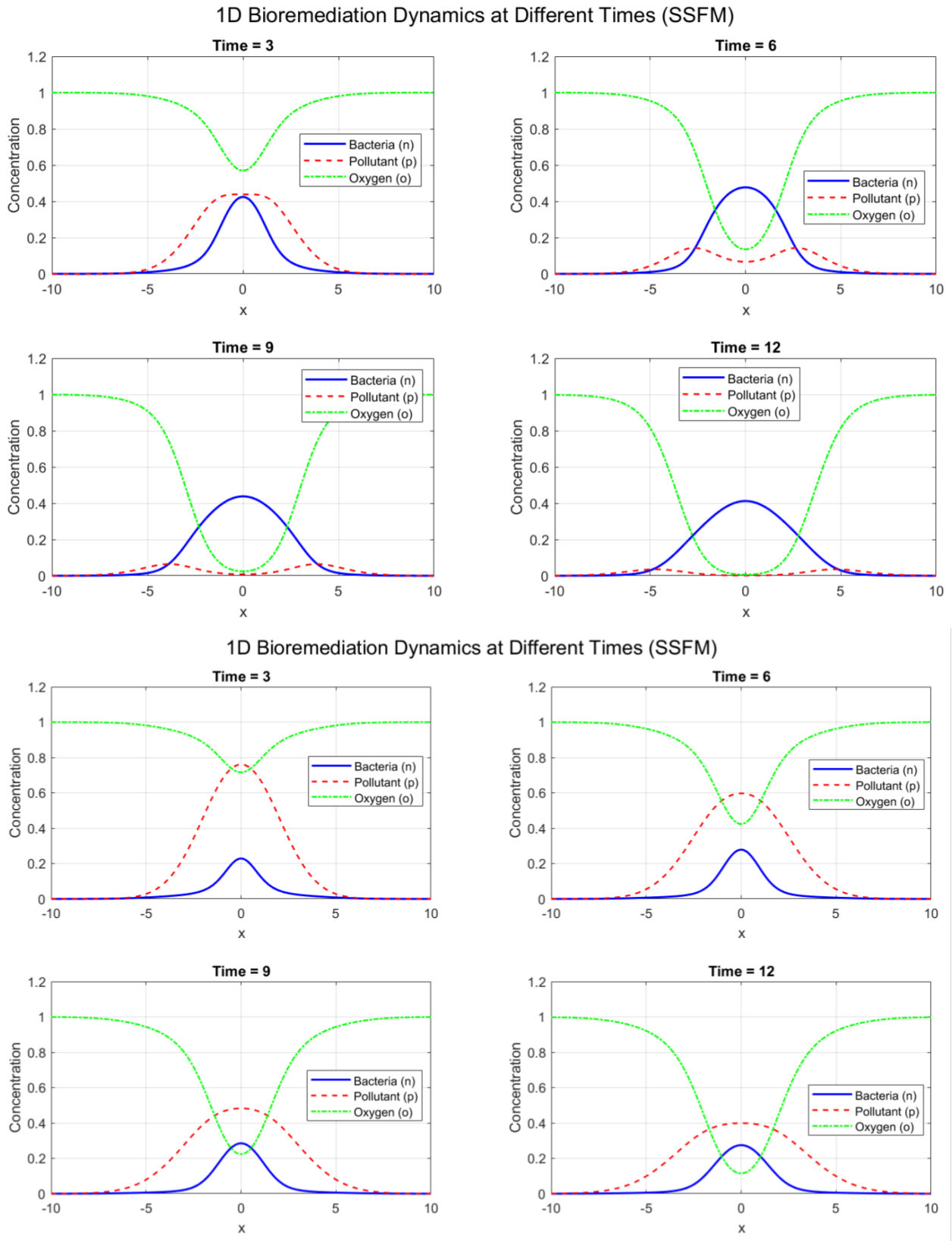

Figure 3. Time evolution of the chemotaxis–reaction model (14) in 1D. Bacterial density $n(x,t)$ (blue), pollutant $p(x,t)$ (red), and oxygen $o(x,t)$ (green) are shown for $T = 3, 6, 9, 12$ in subplots arranged left to right, top to bottom. Bacteria migrate toward the pollutant, aggregate, and consume both the pollutant and oxygen, which results in spatially structured degradation zones. The upper and lower plots correspond to $K_p = 0.5$ and $K_p = 5.0$, respectively.

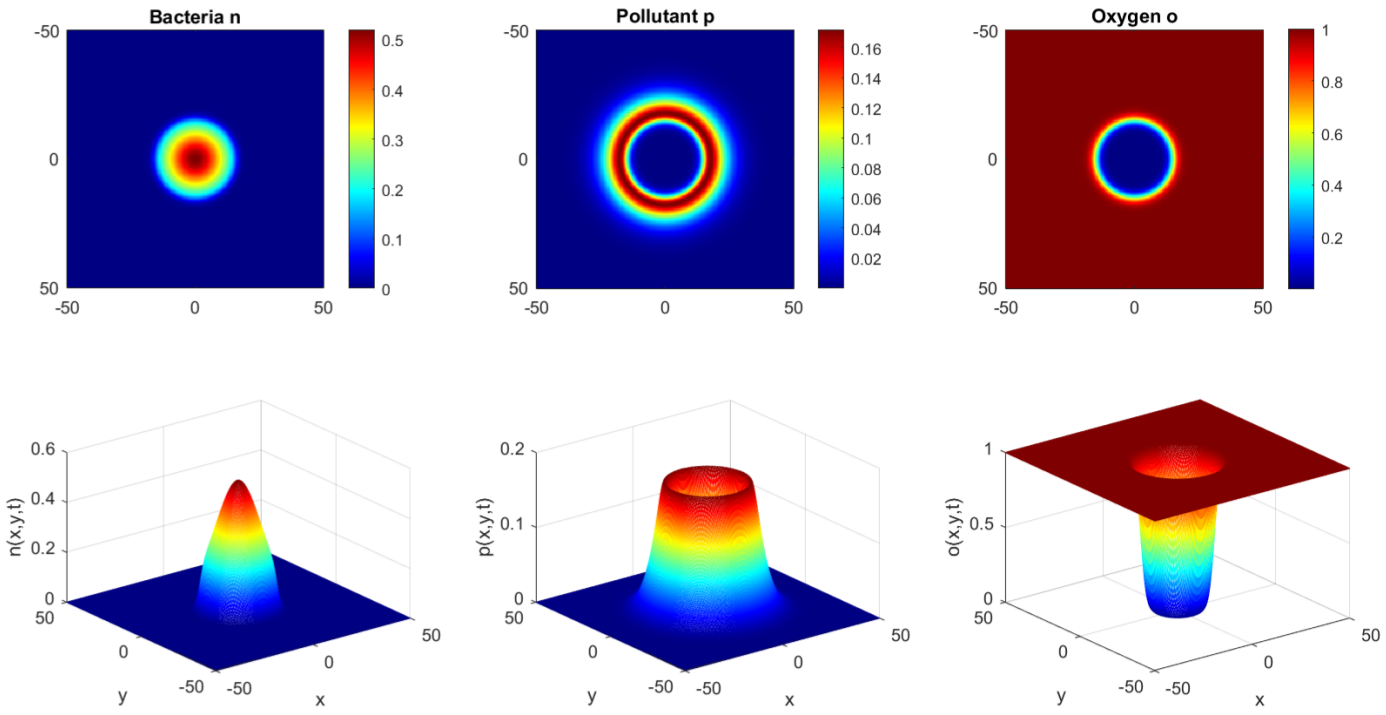

Figure 4. Two-dimensional chemotaxis–reaction dynamics (14) at time $T = 20$. Top row (left to right): Bacterial density $n(x, y)$, pollutant concentration $p(x, y)$, and oxygen concentration $o(x, y)$ shown as 2D color plots. Bottom row: Corresponding 3D mesh plots showing spatial structure of each field. Bacterial density forms a distinct ring as a result of chemotactic aggregation, pollutant degradation, and oxygen depletion.

toward the pollutant, leading to the formation of sharp spatial peaks.
Localized degradation: The pollutant is consumed primarily where bacteria and oxygen co-occur, consistent with a double Monod-type reaction term.
Oxygen limitation: Over time, oxygen is depleted in the central zone, slowing further degradation, which can result in persistent pollutant cores.

These results suggest practical strategies in environmental bioremediation. For example, the emergence of oxygen-limited zones calls for active oxygenation (e.g., air sparging or hydrogen peroxide injection) to ensure continued degradation at the core of the pollutant plume. Furthermore, the observed behavior aligns with ring- or bullseye-shaped bacterial structures often seen in 2D or 3D microbial patterns.

6.5.3 Ring-shaped bioremediation fronts in 2D chemotaxis–reaction systems

To understand spatially resolved biodegradation dynamics, we extended the chemotaxis–reaction model (14) to two spatial dimensions using the Split-Step Fourier Method (SSFM). A radially symmetric initial pollutant field with a Gaussian bacterial distribution was simulated over the square domain $[-50, 50] \times [-50, 50]$. The resulting spatiotemporal evolution is shown in Figure 4, capturing bacterial density $n(x, y, t)$, pollutant $p(x, y, t)$, and oxygen $o(x, y, t)$ at a representative time point $T = 20$.

Ring formation and pattern interpretation. The simulation produces a sharply defined annular structure in the bacterial density, forming a ring centered around the origin. This phenomenon can be explained biologically by the interaction of chemotaxis, nutrient limitation, and spatial diffusion:

Chemotactic migration: Bacteria sense and migrate toward the gradient of the pollutant. Initially concentrated at the center, the pollutant diffuses outward while being consumed by the bacteria. As a result, bacteria move outward toward the expanding front of the pollutant plume, generating the ring-shaped pattern.

Localized growth and depletion: Within the ring, the pollutant and oxygen concentrations fall due to bacterial consumption. However, outside the ring, pollutant and oxygen remain relatively untouched, creating a region where bacterial growth is still favorable. This gradient-driven migration amplifies the ring.

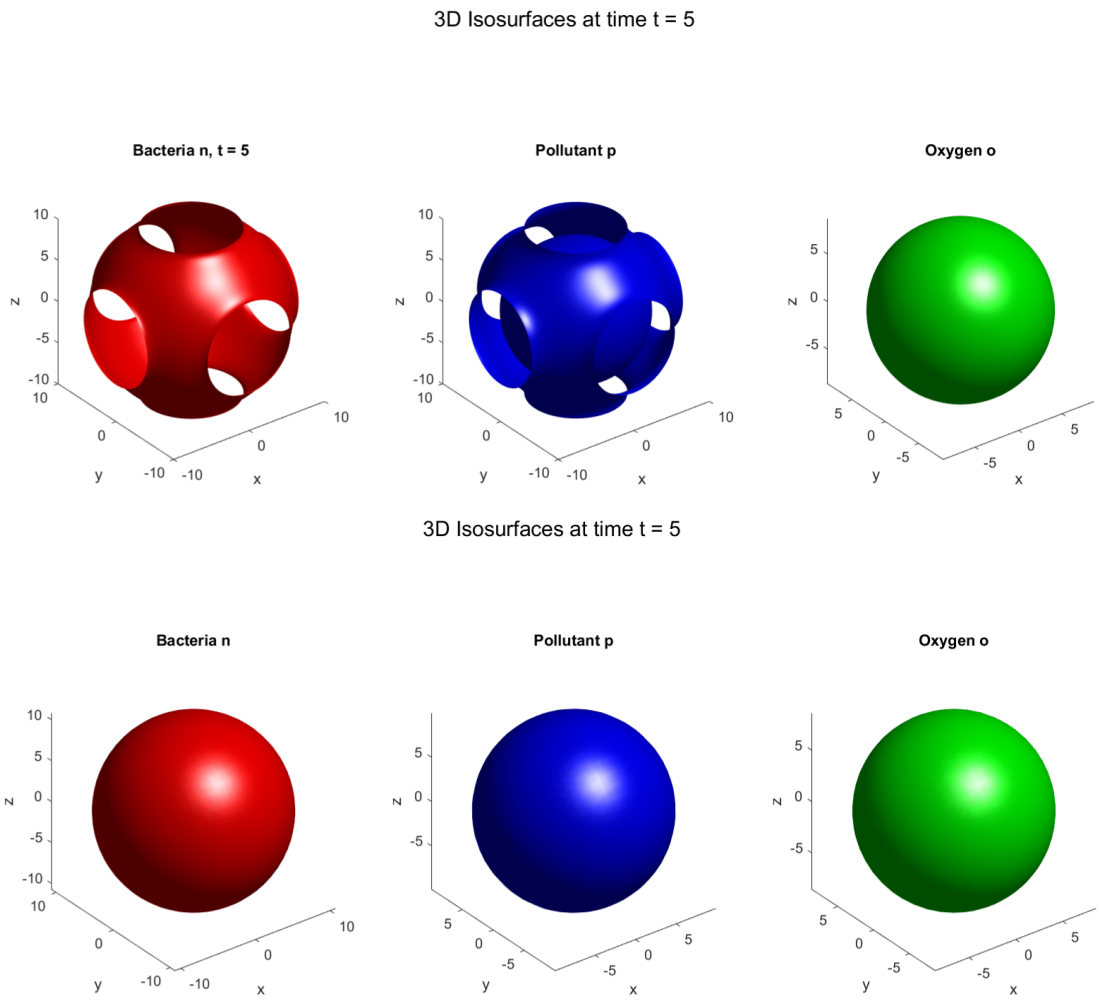

Figure 5. Three-dimensional isosurface plots of the chemotaxis–reaction model at final simulation time $t = 5.0$. The panels show: (column-1) bacterial density $n(x, y, z, t)$ forming localized clusters and ring-like aggregations; (column-2) pollutant concentration $p(x, y, z, t)$ exhibiting depletion in regions of high bacterial activity; and (column-3) oxygen concentration $o(x, y, z, t)$ highlighting areas of significant metabolic consumption. The isosurfaces were computed at constant threshold levels to emphasize volumetric spatial structures in the evolving scalar fields.

Oxygen limitation: The core region, although initially rich in pollutant, becomes oxygen-depleted, thereby suppressing further bacterial proliferation. This enforces a dynamic exclusion zone at the center and pushes the active growth region outward, reinforcing the ring shape.

Double monod kinetics: The reaction terms incorporate saturable uptake of both pollutant and oxygen. This nonlinear feedback ensures that bacterial growth occurs only in regions where both resources are moderately abundant—spatially selecting the ring zone.

Environmental relevance: Ring-like patterns are reminiscent of microbial colony growth on semi-solid media and biodegradation halos in polluted environments. These emergent zones can be seen as "active fronts" where resource availability, microbial metabolism, and chemotaxis are co-regulating spatial colonization.

Implications. The emergence of ring-shaped fronts underscores the importance of oxygen diffusion in microbial remediation strategies. While bacteria tend to follow pollutant gradients, their long-term viability and degradation capacity are spatially restricted by oxygen availability. Hence, in real-world settings, strategies such as periodic aeration or oxygen-releasing compounds may be necessary to maintain biodegradation efficacy in pollutant hotspots.

This spatial self-organization reflects typical features observed in reaction–diffusion–taxis systems, and provides a platform to model biofilm formation, nutrient-driven migration, and colony morphogenesis under constrained resource dynamics. The

three-dimensional isosurface visualisations (Figure 5) further confirm that these self-organized structures are robust to dimensionality and capture the volumetric interplay between bacterial aggregation, pollutant degradation, and metabolic oxygen consumption.

Discussion of 3D Isosurface Results

Also in this study, we implemented a three-dimensional simulation of a chemotaxis–reaction model (14) involving the spatial dynamics of bacterial density $n(x, y, z, t)$, pollutant concentration $p(x, y, z, t)$, and oxygen availability $o(x, y, z, t)$. The model was solved numerically using the Split-Step Fourier Method (SSFM) with periodic boundary conditions. To effectively visualize the spatiotemporal dynamics, we employed isosurface plots, which reveal geometric structures in scalar fields at constant threshold values over time.

The isosurfaces for the bacterial density n provide critical insight into the spatial self-organization of microorganisms under nutrient and oxygen gradients. Initially, the bacteria are symmetrically distributed near the center due to a Gaussian initial condition. As time progresses, the bacteria exhibit directional migration and aggregation behavior, forming localized clusters and filament-like patterns. These patterns emerge as a direct consequence of chemotactic movement toward higher concentrations of the pollutant p, which acts as a chemoattractant, and are further modulated by oxygen availability.

The isosurface visualization of the pollutant p shows a complementary behavior to that of the bacterial density. Regions with initially high pollutant concentration gradually diminish in intensity as bacteria consume the pollutant during growth and chemotactic movement. The resulting spatial depletion zones often correspond to the high-density bacterial regions, thus indicating an inverse spatial correlation between n and p as the system evolves.

The oxygen concentration o displays a more diffuse and slowly evolving isosurface structure, owing to the lower consumption rate and higher diffusion coefficient. However, regions of significant oxygen depletion emerge over time, particularly in zones with elevated bacterial concentration. This further highlights the role of oxygen as a secondary but critical regulator of bacterial dynamics in three dimensions.

The 3D isosurfaces also reveal spatial anisotropy and structural heterogeneity that are not visible in 2D simulations. For instance, the bacteria form layered or shell-like aggregations along certain directions, which may be linked to nonlinear interactions between chemotaxis and diffusion. These volumetric structures are reminiscent of pattern formation phenomena observed in microbial ecology, such as biofilm stratification and ring colony growth in gel media.

Overall, the 3D isosurface representations offer a powerful tool for interpreting the complex feedback between taxis, resource consumption, and spatial constraints. Such results are essential for understanding realistic biological phenomena where environmental heterogeneity and dimensionality play crucial roles.

3D spatial dynamics of bacterial concentration

Figure 6 illustrates the three-dimensional isosurface distribution of the bacterial population $n(x, y, z, t)$ at the final simulation time $t = 2$, computed over a discretized domain with $N_x = N_y = N_z = 5$ grid points. Due to the coarse resolution, the spatial structures are represented by distinct volumetric clusters, giving the appearance of molecular-like aggregations within the bounded computational cube.

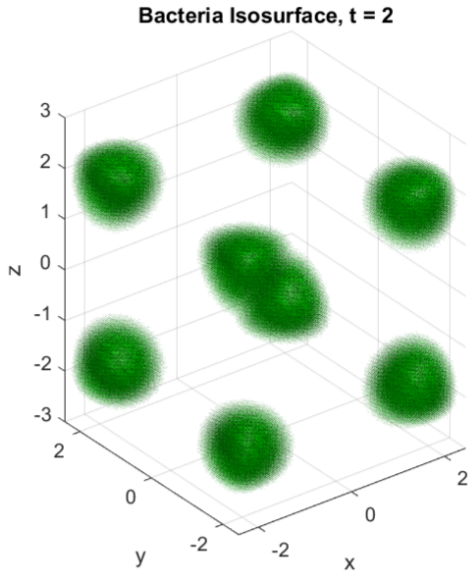

Figure 6. Three-dimensional isosurface representation of the bacterial concentration $n(x, y, z, t)$ at time $t = 2$, using a grid resolution of $N_x = N_y = N_z = 5$. Distinct clusters of bacteria are observed, resembling molecular-like structures isolated within the computational domain. This reflects localized chemotactic aggregation driven by nutrient and oxygen availability.

Biologically, this isolated spatial configuration reflects the early-stage patterning in bacterial chemotaxis under nutrient-driven migration and oxygen consumption. The bacteria tend to localize in

regions where both nutrient and oxygen are relatively abundant, leading to high-density pockets, while surrounding regions remain sparsely populated. Such localized behavior is consistent with the formation of bacterial microcolonies or early biofilm nucleation events observed in confined or structured environments [1, 35].

The isosurface structures suggest that, even under low-resolution constraints, the chemotactic feedback is sufficient to drive nonuniform aggregation. The separation between clusters also hints at inhibitory interactions or spatial resource competition, preventing a uniform spread. These emergent dynamics are crucial in understanding microbial bioremediation strategies, where bacterial motility is guided by pollutant gradients in three-dimensional porous media [55].

Future simulations at higher spatial resolution will reveal whether these isolated bacterial islands evolve into continuous ring-like fronts or remain as localized colonies, and will better resolve the interplay between chemotaxis, diffusion, and nutrient consumption.

7 Open Problems and Future Directions

Chemotaxis plays a fundamental role in a wide range of biological, ecological, and biomedical processes, motivating extensive mathematical modeling and computational studies. Recent works have demonstrated its applications in collective motion, microbial organization, tumor progression, and ecological pattern formation. For example, decentralized gathering and navigation in heterogeneous environments with obstacles were investigated through multi-agent chemotaxis models in [56], while cell aggregation and clustering driven by chemical signaling were analyzed in [57]. In biomedical contexts, chemotactic mechanisms have been incorporated into vascular tumor growth models to better understand cancer invasion and tissue dynamics [58]. Chemotaxis also plays an important role in ecological interactions and social insect behavior, such as ant territory formation mediated by pheromone signaling and alarm responses [59]. From a theoretical perspective, the enhancement of reaction processes through flux-limited chemotaxis has been rigorously studied in [60], revealing how directed movement can significantly alter reaction dynamics. At the microbiological scale, bacterial motility and adaptation mechanisms governed by chemotaxis continue to provide insight into physiological and molecular processes [61]. Furthermore, chemotaxis-related biomarkers are increasingly being explored for clinical applications, particularly in cancer prognosis, where neutrophil chemotaxis scores and associated genes have shown predictive potential for patient survival outcomes [62].

Chemotaxis–reaction modeling has advanced significantly, but numerous challenges and opportunities remain. We highlight some open problems and possible future research directions that are currently at the forefront of this field:

Stochastic and noisy chemotactic behavior. Traditional models use deterministic PDEs and assume large numbers of cells. However, in many scenarios (e.g., early infection when only a few bacteria are present, or microfluidic experiments tracking single cells), fluctuations and randomness are important. Stochastic chemotaxis models, such as stochastic differential equations (for individual cell trajectories) or stochastic PDEs (adding noise terms to concentrations), are an active area. One open question is how noise influences pattern formation: does randomness disrupt patterns or perhaps initiate them (by serving as a perturbation that triggers an instability)? Mathematically, the analysis of stochastic chemotaxis equations is quite challenging, and few results exist on their long-time behavior or pattern probabilities. Developing techniques to rigorously handle noise (e.g., via probabilistic coupling or large deviation theory) could bridge the gap between single-cell behavior and continuum predictions. From the applied side, incorporating variability in cell responses (phenotypic heterogeneity) into models is important. Real bacteria are not identical; some may not respond strongly to attractant, others might have different swimming speeds. Models that include distributions of behaviors (perhaps via population balance equations or interacting particle systems) could provide more realistic forecasts of community behavior.

Multiscale modeling from molecules to populations. Chemotaxis spans multiple scales: internally, molecular interactions (ligand binding to receptors, signaling cascades controlling flagellar motors) govern how a cell decides to turn or run; externally, those decisions accumulate to produce population movement patterns. Deriving continuum models from microscopic descriptions is an ongoing pursuit. There has been progress using kinetic theory (velocity-jump processes and diffusion approximations) [38], but

many derivations assume simple conditions (e.g. shallow gradients, independent cells). Incorporating more detailed molecular models of chemotactic sensing (which may include receptor saturation, adaptation mechanisms, etc.) into population-level equations is an open problem. It may require new intermediate models like hybrid agent-field models or hierarchical homogenization techniques. The reward would be models with parameters directly tied to measurable cellular properties (like receptor sensitivity), improving predictive power. Additionally, linking scales could help understand how microscale constraints (like physical size of cells or sensory noise at low molecule counts) set fundamental limits on macroscale pattern formation (e.g., minimum size of an aggregation, or maximum gradient sensing distance).

Integration with experimental and omics data. With modern experimental techniques, we can measure many aspects of microbial systems: gene expression profiles (transcriptomics), protein levels (proteomics), metabolite concentrations (metabolomics), and spatial structure via advanced imaging. A future direction is to integrate these data types with chemotaxis–reaction models. For instance, RNA sequencing might reveal upregulation of certain chemotaxis genes under some conditions, suggesting an enhanced χ value in the model for those conditions. One open challenge is parameter inference: given spatiotemporal data of cell density and chemical concentrations (from fluorescent reporters, say), can we fit model parameters (diffusivities, sensitivities, reaction rates) robustly? This becomes complex if the model has many parameters or if data are noisy/incomplete. Techniques from data assimilation and machine learning might be employed to calibrate models. Conversely, models can help interpret high-dimensional data: e.g. a model might predict that a certain pattern is due to chemotaxis to a nutrient, which could then be checked by seeing if genes for nutrient chemotaxis are enriched in the dataset.

Moreover, new experimental setups like microfluidic devices allow precise control of chemical gradients in space and time. We can impose arbitrarily shaped attractant fields and see how bacteria respond. This opens the possibility of quantitatively testing model predictions (for example, verifying the functional form of the chemotactic flux term, or measuring the critical mass for aggregation in a controlled way). Models will need to be adapted to these specific geometries (often microchannels or chambers) and to include boundary effects (e.g. bacteria accumulating at walls). Ensuring models can simulate these experimental designs will create a tight model-experiment feedback loop.

Machine learning and data-driven model inference. The rise of machine learning provides new tools to study chemotaxis systems. One direction is using neural networks or other ML methods to discover effective equations from data. For example, if we simulate an agent-based model of chemotaxis or gather high-resolution experimental data, can a neural network automatically infer the PDE that describes it (including, say, the fact that the flux is $-\chi n \nabla c$)? Some initial works using techniques like PDE-net or symbolic regression have shown success in simpler biological patterning contexts; applying these to chemotaxis could reveal whether the classical forms are the only ones or if, under certain conditions, nonstandard terms appear.

Another application of ML is in accelerating simulations and analysis. Surrogate models (e.g. a trained network that predicts pattern outcomes without solving the PDE each time) could allow rapid exploration of parameter space. This might assist in solving inverse problems: given an observed pattern, find which parameters (or which model among many) likely produced it. Evolutionary algorithms or Bayesian optimization can also be coupled with simulations to design experiments or optimize biological systems. For instance, one could ask: what chemotactic sensitivity should a engineered bacterium have to best colonize a particular tumor tissue (for cancer therapy)? By treating the model as a black box and using optimization algorithms, one can arrive at answers that guide synthetic biology efforts.

Lastly, there is interest in controlling chemotactic systems. With light-sensitive ion channels and optogenetics, researchers can now remotely control cell signaling (including chemotaxis pathways) with light. A control theory problem emerges: how to shine light (spatially and temporally) to steer an aggregation to a desired location or to disperse a harmful biofilm? This falls under optimal control of PDEs with chemotaxis. Early theoretical work is examining controllability (can we drive the system from one state to another with an input function?) and optimal control (minimize a cost, e.g. time or energy, to achieve a configuration). This is quite open, as chemotaxis PDEs are nonlinear and the control enters in nonlinear ways (e.g. as an added term in the chemical equation representing light-induced attractant release). Techniques from control theory

combined with numerical adjoint methods could pave the way for guiding microbial patterns, which has potential applications in bioprinting and targeted therapy.

In conclusion, the future of chemotaxis–reaction modeling is highly interdisciplinary. It will involve advanced mathematics (stochastic analysis, multi-scale asymptotics, control theory), integration with cutting-edge experiments (microfluidics, omics), and modern computational tools (HPC simulations, machine learning). The ultimate goal is not only to understand microbial behavior in nature but also to harness and direct it in technological and medical contexts. The open problems listed here represent stepping stones toward that vision.

8 Conclusion

Chemotaxis–reaction models continue to provide a fundamental mathematical framework for understanding the collective behavior of microbial populations and the emergence of complex spatial organization in biological systems. Throughout this review, we have demonstrated how the interplay between chemotactic transport, diffusion, nonlinear reactions, and ecological interactions generates a broad spectrum of dynamical phenomena, including aggregation, traveling bands, wave propagation, biofilm organization, chaotic oscillations, and large-scale pattern formation. The combination of rigorous PDE analysis, numerical simulation, and experimental observation has substantially advanced our understanding of these systems and clarified the mechanisms responsible for boundedness, instability, bifurcation, and self-organization.

A central theme emerging from this survey is that biologically relevant dynamics arise from delicate balances between competing mechanisms, including diffusion versus directed migration, growth versus saturation, attraction versus repulsion, and cooperation versus competition. Mathematical analysis has identified critical thresholds governing transitions between homogeneous states, stable patterns, and blow-up behavior, while computational studies have revealed highly nonlinear regimes that remain analytically inaccessible. At the same time, experimental advances in microbial imaging, microfluidics, and high-throughput biological measurements have increasingly enabled quantitative validation of chemotaxis models and more realistic parameter estimation.

Despite significant progress, several important challenges remain open and will likely shape future research directions in the field. One major challenge concerns the incorporation of stochasticity and heterogeneity into chemotaxis models. Classical deterministic PDE systems often neglect fluctuations arising from low population densities, environmental variability, and phenotypic diversity among cells. Developing mathematically tractable stochastic and hybrid frameworks capable of capturing both single-cell variability and population-level organization remains an important open problem.

Another critical direction involves multiscale modeling. Chemotactic behavior originates from intracellular biochemical signaling processes, yet most continuum models describe only macroscopic population dynamics. Establishing rigorous links between molecular signaling pathways, kinetic transport descriptions, and continuum PDE formulations remains incomplete. Future progress will require improved multiscale derivations, hybrid particle–continuum formulations, and models capable of simultaneously resolving cellular and ecological scales.

The integration of chemotaxis models with experimental and omics data also represents a major frontier. Modern biological experiments now generate highly resolved spatial and temporal datasets, including transcriptomic, proteomic, and metabolomic information. However, robust parameter inference, uncertainty quantification, and model calibration for high-dimensional chemotaxis systems remain challenging. Data assimilation techniques, inverse problems, and machine-learning-assisted parameter estimation are therefore expected to play an increasingly important role in future studies.

Machine learning and scientific artificial intelligence offer additional opportunities for accelerating simulations, discovering effective reduced-order models, and identifying governing equations directly from experimental observations. Data-driven approaches may also improve model selection, optimize parameter exploration, and assist in the design of controlled chemotactic systems for biomedical and environmental applications. Nevertheless, ensuring physical consistency, interpretability, and mathematical reliability of such approaches remains an important unresolved issue.

Another promising research direction concerns the

optimal control and manipulation of chemotactic systems. Advances in optogenetics, synthetic biology, and programmable microbial engineering raise new questions regarding the controllability of chemotactic populations and the design of external signals capable of steering aggregation, suppressing harmful biofilms, or enhancing targeted transport. These problems naturally connect chemotaxis modeling with control theory, optimization, and biomedical engineering.

Overall, the future of chemotaxis–reaction modeling will depend increasingly on interdisciplinary collaboration between mathematics, computation, biology, physics, and data science. Many theoretical questions concerning global dynamics, singularity formation, stochastic effects, and multiscale coupling remain unresolved, while emerging experimental technologies continue to reveal increasingly complex microbial behaviors that challenge existing models. Addressing these open problems will not only deepen our understanding of microbial ecology and self-organization but may also enable new technological applications involving engineered microbial systems, targeted therapeutic delivery, environmental remediation, and synthetic biological design. Chemotaxis–reaction models therefore remain both a rich mathematical subject and a powerful scientific framework for investigating and controlling collective biological dynamics.

Data Availability Statement

Data will be made available on request.

Funding

This work was supported without any funding.

Conflicts of Interest

The authors declare no conflicts of interest.

AI Use Statement

The authors declare that no generative AI was used in the preparation of this manuscript.

Ethical Approval and Consent to Participate

Not applicable.

References

[1] Adler, J. (1966). Chemotaxis in Bacteria: Motile Escherichia coli migrate in bands that are influenced by oxygen and organic nutrients. *Science, 153*(3737), 708-716. [CrossRef]

[2] Keller, E. F., & Segel, L. A. (1971). Model for chemotaxis. *Journal of theoretical biology, 30*(2), 225-234. [CrossRef]

[3] Hillen, T., & Painter, K. J. (2009). A user's guide to PDE models for chemotaxis. *Journal of mathematical biology, 58*(1), 183-217. [CrossRef]

[4] Painter, K. J. (2019). Mathematical models for chemotaxis and their applications in self-organisation phenomena. *Journal of theoretical biology, 481*, 162-182. [CrossRef]

[5] Winkler, M. (2010). Boundedness in the higher-dimensional parabolic-parabolic chemotaxis system with logistic source. *Communications in Partial Differential Equations, 35*(8), 1516-1537. [CrossRef]

[6] Wang, Z. (2013). Mathematics of traveling waves in chemotaxis-Review paper. *Discrete and Continuous Dynamical Systems-Series B, 18*(3), 601-641. [CrossRef]

[7] Owolabi, K. M., Mare, E., Ijalana, C. O., & Adegbie, K. S. (2026). Multi-Species Keller–Segel Systems: Analysis, Pattern Formation, and Emerging Mathematical Structures. *arXiv preprint arXiv:2603.04931*. [CrossRef]

[8] Keller, E. F., & Segel, L. A. (1971). Traveling bands of chemotactic bacteria: a theoretical analysis. *Journal of theoretical biology, 30*(2), 235-248. [CrossRef]

[9] Bellomo, N., Bellouquid, A., Tao, Y., & Winkler, M. (2015). Toward a mathematical theory of Keller–Segel models of pattern formation in biological tissues. *Mathematical Models and Methods in Applied Sciences, 25*(09), 1663-1763. [CrossRef]

[10] Horstmann, D. (2003). *From 1970 until present: The Keller-Segel model in chemotaxis and its consequences* (Preprint No. 3). Max-Planck-Institut für Mathematik in den Naturwissenschaften Leipzig. https://webdoc.sub.gwdg.de/ebook/serien/e/MPI_Math_Nat/preprint2003_3.pdf

[11] Perthame, B. (2007). *Transport Equations in Biology*. Birkhäuser. [CrossRef]

[12] Winkler, M. (2010). Aggregation vs. global diffusive behavior in the higher-dimensional Keller–Segel model. *Journal of Differential Equations, 248*(12), 2889-2905. [CrossRef]

[13] Fuest, M. (2020). Finite-time blow-up in a two-dimensional Keller–Segel system with an environmental dependent logistic source. *Nonlinear Analysis: Real World Applications, 52*, 103022. [CrossRef]

[14] Tao, Y., & Winkler, M. (2012). Boundedness in a quasilinear parabolic–parabolic Keller–Segel system with subcritical sensitivity. *Journal of Differential Equations, 252*(1), 692-715. [CrossRef]

[15] Arumugam, G., & Tyagi, J. (2021). Keller-Segel chemotaxis models: a review. *Acta Applicandae Mathematicae, 171*(1), 6. [CrossRef]

[16] Fraga Delfino Kunz, C., Gerisch, A., Glover, J., Headon, D., Painter, K. J., & Matthäus, F. (2024). Novel aspects in pattern formation arise from coupling turing reaction–diffusion and chemotaxis. *Bulletin of Mathematical Biology, 86*(1), 4. [CrossRef]

[17] Cremer, J., Honda, T., Tang, Y., Wong-Ng, J., Vergassola, M., & Hwa, T. (2019). Chemotaxis as a navigation strategy to boost range expansion. *Nature, 575*(7784), 658-663. [CrossRef]

[18] Wadhams, G. H., & Armitage, J. P. (2004). Making sense of it all: bacterial chemotaxis. *Nature reviews Molecular cell biology, 5*(12), 1024-1037. [CrossRef]

[19] Raina, J. B., Lambert, B. S., Parks, D. H., Rinke, C., Siboni, N., Bramucci, A., ... & Seymour, J. R. (2022). Chemotaxis shapes the microscale organization of the ocean's microbiome. *Nature, 605*(7908), 132-138. [CrossRef]

[20] Narla, A. V., Cremer, J., & Hwa, T. (2021). A traveling-wave solution for bacterial chemotaxis with growth. *Proceedings of the National Academy of Sciences, 118*(48), e2105138118. [CrossRef]

[21] Chertock, A., Kurganov, A., Ricchiuto, M., & Wu, T. (2019). Adaptive moving mesh upwind scheme for the two-species chemotaxis model. *Computers & Mathematics with Applications, 77*(12), 3172-3185. [CrossRef]

[22] Xue, C., & Othmer, H. G. (2009). Multiscale models of taxis-driven patterning in bacterial populations. *SIAM Journal on Applied Mathematics, 70*(1), 133-167. [CrossRef]

[23] Budrene, E. O., & Berg, H. C. (1991). Complex patterns formed by motile cells of *Escherichia coli*. *Nature, 349*(6310), 630–633. [CrossRef]

[24] Blanchet, A., Dolbeault, J., & Perthame, B. (2006). Two-dimensional Keller-Segel model: optimal critical mass and qualitative properties of solutions. *Electronic Journal of Differential Equations, 2006*(44), 1-33. https://eudml.org/doc/127363

[25] Tello, J. I., & Winkler, M. (2007). A chemotaxis system with logistic source. *Communications in Partial Differential Equations, 32*(6), 849–877. [CrossRef]

[26] Issa, T. B., & Shen, W. (2019). Persistence, coexistence and extinction in two species chemotaxis models on heterogeneous environments. *Journal of Dynamics and Differential Equations, 31*(4), 1839–1871. [CrossRef]

[27] Issa, T. B., & Shen, W. (2019). Uniqueness and stability of coexistence states in two species models with/without chemotaxis on bounded heterogeneous environments. *Journal of Dynamics and Differential Equations, 31*(4), 2305-2338. [CrossRef]

[28] Tuval, I., Cisneros, L., Dombrowski, C., Wolgemuth, C. W., Kessler, J. O., & Goldstein, R. E. (2005). Bacterial swimming and oxygen transport near contact lines. *Proceedings of the National Academy of Sciences, 102*(7), 2277-2282. [CrossRef]

[29] Winkler, M. (2012). Global large-data solutions in a chemotaxis-(Navier–) Stokes system modeling cellular swimming in fluid drops. *Communications in Partial Differential Equations, 37*(2), 319-351. [CrossRef]

[30] Keegstra, J. M., Carrara, F., & Stocker, R. (2022). The ecological roles of bacterial chemotaxis. *Nature Reviews Microbiology, 20*(8), 491-504. [CrossRef]

[31] Brumley, D. R., Carrara, F., Hein, A. M., Hagstrom, G. I., Levin, S. A., & Stocker, R. (2020). Cutting through the noise: bacterial chemotaxis in marine microenvironments. *Frontiers in Marine Science, 7*, 527. [CrossRef]

[32] Jeong, H. H. (2021). Recent developments in bacterial chemotaxis analysis based on the microfluidic system. *SLAS TECHNOLOGY: Translating Life Sciences Innovation, 26*(2), 159-164. [CrossRef]

[33] Zhao, X., & Gao, B. (2026). AI and Microfluidics: Unlocking Cellular Motility for Bioengineering. *Bioengineering, 13*(2), 172. [CrossRef]

[34] Jäger, W., & Luckhaus, S. (1992). On explosions of solutions to a system of partial differential equations modelling chemotaxis. *Transactions of the american mathematical society, 329*(2), 819-824. [CrossRef]

[35] Budrene, E. O., & Berg, H. C. (1995). Dynamics of formation of symmetrical patterns by chemotactic bacteria. *Nature, 376*(6535), 49-53. [CrossRef]

[36] Patlak, C. S. (1953). Random walk with persistence and external bias. *The bulletin of mathematical biophysics, 15*(3), 311-338. [CrossRef]

[37] Alt, W. (1980). Biased random walk models for chemotaxis and related diffusion approximations. *Journal of mathematical biology, 9*(2), 147-177. [CrossRef]

[38] Stevens, A., & Othmer, H. G. (1997). Aggregation, blowup, and collapse: the ABC's of taxis in reinforced random walks. *SIAM Journal on Applied Mathematics, 57*(4), 1044-1081. [CrossRef]

[39] Painter, K. J., & Hillen, T. (2011). Spatio-temporal chaos in a chemotaxis model. *Physica D: Nonlinear Phenomena, 240*(4-5), 363-375. [CrossRef]

[40] Owolabi, K. M., Pindza, E., & Jain, S. (2025). Complex spatiotemporal phenomena in multi-dimensional reaction–diffusion system. *The European Physical Journal Special Topics, 234*(8), 2565-2599. [CrossRef]

[41] Cox, S. M., & Matthews, P. C. (2002). Exponential time differencing for stiff systems. *Journal of Computational Physics, 176*(2), 430-455. [CrossRef]

[42] Kassam, A. K., & Trefethen, L. N. (2005). Fourth-order time-stepping for stiff PDEs. *SIAM Journal on Scientific Computing, 26*(4), 1214-1233. [CrossRef]

[43] Boyd, J. P. (2001). *Chebyshev and Fourier spectral methods*. Courier Corporation.

[44] Canuto, C., Hussaini, M. Y., Quarteroni, A., & Zang, T. A. (2006). *Spectral methods*. Berlin: springer. [CrossRef]

[45] Tsimring, L., Levine, H., Aranson, I., Ben-Jacob, E.,

Cohen, I., Shochet, O., & Reynolds, W. N. (1995). Aggregation patterns in stressed bacteria. *Physical review letters, 75*(9), 1859. [CrossRef]

[46] Ben-Jacob, E. (1997). From snowflake formation to growth of bacterial colonies II: Cooperative formation of complex colonial patterns. *Contemporary physics, 38*(3), 205-241. [CrossRef]

[47] Pratt, L. A., & Kolter, R. (1998). Genetic analysis of Escherichia coli biofilm formation: roles of flagella, motility, chemotaxis and type I pili. *Molecular microbiology, 30*(2), 285-293. [CrossRef]

[48] Tao, Y., & Winkler, M. (2022). Existence theory and qualitative analysis for a fully cross-diffusive predator-prey system. *SIAM Journal on Mathematical Analysis, 54*(4), 4806-4864. [CrossRef]

[49] Darrah, P. R. (1991). Models of the rhizosphere: I. Microbial population dynamics around a root releasing soluble and insoluble carbon. *Plant and Soil, 133*(2), 187-199. [CrossRef]

[50] Blackburn, N., Fenchel, T., & Mitchell, J. (1998). Microscale nutrient patches in planktonic habitats shown by chemotactic bacteria. *Science, 282*(5397), 2254-2256. [CrossRef]

[51] Stocker, R. (2012). Marine microbes see a sea of gradients. *science, 338*(6107), 628-633. [CrossRef]

[52] Verwer, J. G., & Sportisse, B. (1998). A note on operator splitting in a stiff linear case. *Report-Modelling, analysis and simulation*, (30), 1-13. http://pascal-francis.inist.fr/vibad/index.php?action=getRecordDetail&idt=1806182

[53] Strang, G. (1968). On the construction and comparison of difference schemes. *SIAM journal on numerical analysis, 5*(3), 506-517. [CrossRef]

[54] Ebert, U., & van Saarloos, W. (2000). Front propagation into unstable states: universal algebraic convergence towards uniformly translating pulled fronts. *Physica D: Nonlinear Phenomena, 146*(1-4), 1-99. [CrossRef]

[55] Kreft, J. U., Picioreanu, C., Wimpenny, J. W., & van Loosdrecht, M. C. (2001). Individual-based modelling of biofilms. *Microbiology, 147*(11), 2897-2912. [CrossRef]

[56] Proverbio, D. (2024). Chemotaxis in heterogeneous environments: A multi-agent model of decentralized gathering past obstacles. *Journal of Theoretical Biology, 586*, 111820. [CrossRef]

[57] Farmer, A., & Harris, P. J. (2023). A mathematical model of cell movement and clustering due to chemotaxis. *Journal of Theoretical Biology, 575*, 111646. [CrossRef]

[58] Arshadi, S., Pishevar, A., Javanbakht, M., & Javanmard, S. H. (2025). Chemotaxis effects on the vascular tumor growth: Phase-field model and simulations. *Mathematical biosciences, 380*, 109366. [CrossRef]

[59] Amorim, P., de Lima, R., & Telch, B. (2025). An ant territory formation model with chemotaxis and alarm pheromones. *Mathematical Biosciences*, 109498. [CrossRef]

[60] An, J., Kiselev, A., & Yao, Y. (2026). Reaction enhancement by flux-limited chemotaxis. *Journal of Mathematical Biology, 92*(4), 57. [CrossRef]

[61] Sharma, I., Nagpal, S., & Mishra, A. K. (2025). Navigating bacterial motility through chemotaxis: from molecular mechanisms to physiological perspectives. *Folia Microbiologica, 70*(4), 753-777. [CrossRef]

[62] Yang, Y., Yang, J., Li, L., Shao, Y., Liu, L., & Sun, B. (2024). Neutrophil chemotaxis score and chemotaxis-related genes have the potential for clinical application to prognosticate the survival of patients with tumours. *BMC cancer, 24*(1), 1244. [CrossRef]